Icarus 220 (2012) 514–529

Contents lists available at SciVerse ScienceDirect

Icarus

journal homepage: www.elsevier.com/locate/icarus

Spin-up of rubble-pile asteroids: Disruption, satellite formation, and equilibrium shapes

Kevin J. Walsh [a,*], Derek C. Richardson [c], Patrick Michel [b]

[a] Southwest Research Institute, 1050 Walnut St., Suite 300, Boulder, CO 80302, USA
[b] University of Nice Sophia Antipolis, CNRS, Observatoire de la Côte d'Azur, B.P. 4229, 06304 Nice Cedex 4, France
[c] Department of Astronomy, University of Maryland, College Park, MD 20742, USA

ARTICLE INFO

Article history:
Received 3 April 2012
Accepted 28 April 2012
Available online 18 May 2012

Keywords:
Asteroid, Dynamics
Rotational dynamics
Satellites, Dynamics

ABSTRACT

We present results from numerical experiments testing the behavior of cohesionless gravitational aggregates experiencing a gradual increase of angular momentum. The test bodies used in these numerical simulations are gravitational aggregates of different construction, distinguished by the size distribution of the particles constituting them, parameterized in terms of the angle of friction (ϕ). Shape change and mass loss are found to depend strongly on ϕ, with results ranging from oblate spheroids forming binary systems to near-fluid behavior characterized by mass shedding bursts and no binary formation. Bodies with the highest angle of friction, $\phi \sim 40°$, evolve to shapes with average axis ratios of $c/a \sim 0.70$ and $b/a \sim 0.90$ ($a \geqslant b \geqslant c$), and are efficient at forming satellites. Bodies with lower angle of friction, $\phi \sim 20°$, evolve to shapes with average axis ratios of $c/a \sim 0.61$ and $b/a \sim 0.83$, and are less efficient at forming satellites. The most fluid-like bodies tested, with ϕ near zero, become very elongated, with average axis ratios $c/a \sim 0.40$ and $b/a \sim 0.56$, and do not form satellites in any simulation. In all but 2 fluid-like cases out of 360, no more than 5% of the total mass was ejected in a single event. Bodies with substantial cores were also tested under slow spin-up, and cases with cores larger than ~30% of the total mass were successful at forming binaries.

The binary systems created in all simulations are analyzed and compared against observed binary near-Earth asteroids and small Main Belt asteroids. The shape and rotation period of the primary, orbital and rotational period of the secondary, and the orbital semi-major axis and eccentricity are found to closely match the observed population.

© 2012 Elsevier Inc. All rights reserved.

1. Introduction

The equilibrium shape that a deformable body will take for a given spin depends on the internal structure of the body (see e.g., Holsapple, 2007). It is well known that beyond a certain rotation rate, which depends on a number of physical parameters, the body cannot maintain its original state. It must either adjust to another shape, or lose mass. The limiting rotation rate depends on the body's internal structure and the behavior of its constituent material.

This is directly applicable to asteroids in the Solar System, as studies have shown that many undergo substantial spin-state changes over their lifetimes. Specifically, asteroids referred to as "rubble piles" – seemingly strengthless aggregates that are held together only by their constituents' self-gravity – are of particular interest as they may re-shape and shed mass if pushed to rapid rotation rates. Thus a direct study of the evolution of "rubble pile" asteroids under slow rotational spinup will relate to the observed properties of small asteroids.

1.1. The YORP effect

A natural mechanism widely attributed with imparting spin-state changes on small bodies is the YORP effect, which arises from reflection and/or absorption and re-emission of solar radiation by the surface of an irregularly shaped asteroid (Rubincam, 2000; Paddack and Rhee, 1975; Bottke et al., 2006). This effect has been identified as the cause of rotation-rate increase of NEAs (54509) 2000 PH5 (later named 54509 YORP in recognition of the direct detection, Taylor et al., 2007), (1862) Apollo (Lowry et al., 2007; Kaasalainen et al., 2007) and (1620) Geographos (Durech et al., 2008). It has also been observed to change the obliquity and rotation rates in a subset of Koronis family asteroids (Vokrouhlický et al., 2003; Slivan, 2002).

The timescale for the YORP effect depends on the radius R of the body (increasing with $\approx R^2$), and the distance a from the Sun (increasing with a^2). The magnitude of the effect is also dependent

* Corresponding author.
E-mail address: kwalsh@boulder.swri.edu (K.J. Walsh).

0019-1035/$ - see front matter © 2012 Elsevier Inc. All rights reserved.
http://dx.doi.org/10.1016/j.icarus.2012.04.029

on the body's thermal properties, shape and obliquity. For plausible parameters, the YORP spinup/spindown timescale for kilometer-sized NEAs and MBAs is estimated to be between a few 10^4 and 10^6 years (Rubincam, 2000; Ćuk, 2007). The YORP effect appears to act widely, due to a notable abundance of both fast and slow rotators among NEAs and small MBAs (SMBAs) when compared to larger MBAs (Pravec, 2000; Rubincam, 2000; Pravec et al., 2008; Rossi et al., 2009; Masiero et al., 2009). Given the similar properties of binaries among these small sizes of both NEAs and MBAs, the role of tidal disruption and impacts, which affect NEAs and MBAs in dramatically different ways on different timescales, are both seemingly unimportant (Walsh and Richardson, 2008).

1.2. Equilibrium shapes and granular materials

The spin at which a body disrupts and its subsequent evolution are strongly influenced by the "strengths" of the body's material. These are the tensile, compressive and shear strengths. However, there is strong evidence that asteroids with sizes above a few hundreds of meters are likely to be cohesionless, meaning a lack of tensile strength (Harris, 1996; Richardson et al., 2002; Pravec et al., 2008). It is a common mistake to equate "zero tensile strength" with being a fluid body. A granular material such as dry sand can withstand considerable shear stress if it is under pressure, but has no tensile strength. This is why one can walk on dry sand but not on water. Therefore, zero tensile strength does not mean "fluid". The confining pressure, in the case of asteroids, is due to self-gravity. Therefore such a model of a cohesionless body is appropriate for bodies whose gravity dominates over tensile strength. Such bodies are also commonly called rubble piles or gravitational aggregates (see Richardson et al., 2002 for a detailed discussion and definition of gravitational aggregates).

For perfect, self-gravitating, incompressible fluids there is a locus of stable permissible spin and shape combinations. The most relevant and familiar examples are the Maclaurin spheroids and the Jacobi ellipsoids (cf. Binney and Tremaine, 1987). We will follow the convention used in Richardson et al. (2005), by plotting the Maclaurin and Jacobi curves in terms of the axis ratios q_2 and q_3 as a function of the normalized spin frequency (where q_2 is the intermediate axis divided by the long axis, b/a, q_3 is the short over the long axis, c/a, and normalized spin frequency is defined here as $\omega/\sqrt{2\pi G\rho}$). For both curves, the upper segments together describe the Maclaurin spheroids, where q_2 is equal to 1, and q_3 varies as the body becomes increasingly flattened at more rapid rotation (see Figs. 1 and 2). The lower segments describe the Jacobi ellipsoids, where there are unique pairings of q_2 and q_3 at each spin rate.

Holsapple (2001) presented work on cohesionless bodies, detailing shape and spin limits as a function of the Mohr–Coulomb friction angle ϕ. This parameter, ϕ, varies from 0° to 90°, where a body with $\phi = 0°$ is a fluid, and higher values represent materials with some shear strength while under pressure, with normal terrestrial granular materials having $\phi \sim 40°$. This treatment means that for a given body with a non-zero angle of friction there is an envelope of permissible shapes, rather than the locus of points in the classical fluid cases (all relevant fiducials can be seen in Figs. 1 and 2).

Holsapple (2010) used continuum theory to analyze the changes to a self-gravitating ellipsoidal body's shape and spin state during angular momentum increase. Similar models of zero-tensile-strength granular material to those of Holsapple (2001) were used to study the body's response to angular momentum increase. This work has the benefit of creating shape and spin histories for bodies of widely varying angles of friction. It was found that bodies changed their shape without ever experiencing a net outward body force (which is the indication of mass loss in their model). Thus they do not find mass loss or binary formation via gradual angular momentum increase. This model differs from an N-body simulation of a "rubble pile" in that it does not model discrete elements of the bodies, and cannot directly simulate mass loss (though it can estimate if any part of the surface has a net outward force). The seeming contradiction between the approaches

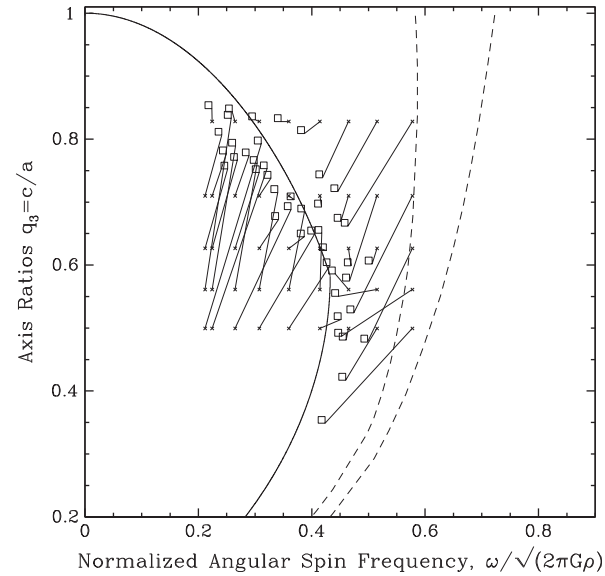

Fig. 1. The results of spin-limit tests for the "fluid" rubble pile, created with a bimodal size distribution of particles. The small crosses are the starting points of the rubble piles, and the lines connect to the open squares, which are located where the rubble piles ended after evolving. The vertical axis is the c/a axis ratio of the rubble pile and it is plotted against the normalized angular spin frequency. The solid line is the Maclaurin/Jacobi fiducial for the c/a axis and the dashed lines are the analytical limits for the frictionless granular material with angles of friction of 20° (left) and 40° (right).

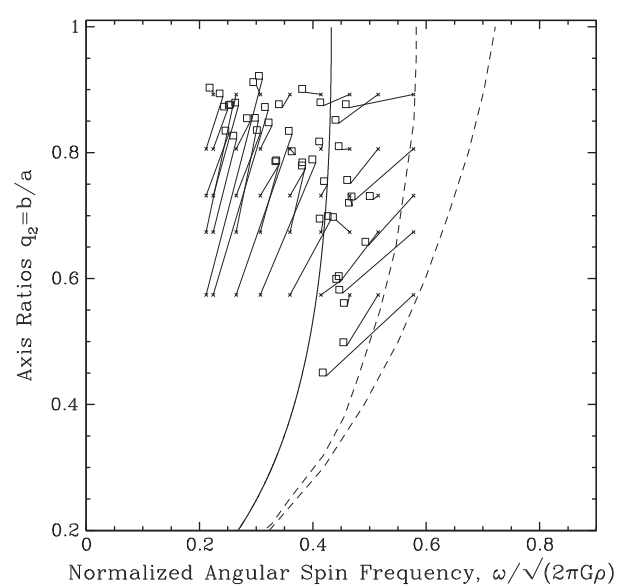

Fig. 2. The results of spin-limit tests for the "fluid" rubble pile, created with a bimodal size distribution of particles. The small crosses are the starting points of the rubble piles, and the lines connect to the open squares, which are located where the rubble piles ended after evolving. The vertical axis is the b/a axis ratio of the rubble pile and it is plotted against the normalized angular spin frequency. The solid line is the Maclaurin/Jacobi fiducial for the b/a axis and the dashed lines are the analytical limits for the frictionless granular material with angles of friction of 20° (left) and 40° (right).

may be explained by the discrete nature of the N-body simulations, a topic we will return to throughout this paper.

1.3. Binary asteroid population

An important motivation of this work was the investigation of possible formation mechanisms of binary asteroids. Among small asteroids, both NEAs and MBAs smaller than 10 km, there is a high fraction of binary systems that share similar properties (~15%). A common formation mechanism is suggested due to these following properties of the binaries:

- Rapidly rotating primaries, with rotation rates between 2.2–4 h.
- Close, moderately-sized secondaries (20–50% the size of the primary), typically orbiting within 5 primary radii.
- Nearly spherical or oblate primaries – possibly "top-shaped" like 1999 KW_4.

Tidal disruption by a terrestrial planet was investigated as a possible formation mechanism, but was found to not reproduce all of the properties, such as primary shape and low-eccentricity orbits (Richardson et al., 1998; Walsh and Richardson, 2006, 2008). Similarly, recent discoveries of these types of binaries in the Main Belt, where there are no possible disruptive tidal interactions, suggests a rotational disruption mechanism other than tidal disruption (Pravec and Harris, 2007). Around 15% of NEAs and small MBAs are estimated to be binaries, hence the responsible formation mechanism is something that is widespread, and generic – creating a population of binaries that have very similar properties.

Some of the results in this study directly follow on from the investigation of binary formation presented in Walsh et al. (2008). This work found that spin-up is a viable binary formation mechanism that re-created many of the properties of the observed systems. Here we provide more detail on this work and present new results from our numerical experiments.

2. Methods

Many of the simulation parameters used in this work can be found in the literature (e.g Richardson et al., 2000). However, this work also constrains results as a function of the body's material properties, specifically the estimated angle of friction of the specific test body. We have taken our model asteroids, compared their re-shaping behavior to analytical formulations and determined an approximate angle of friction. This is the first time this has been done for these applications and the construction of the model asteroids and the testing of their behavior is described below in detail. Similarly, the spin-up mechanism was created specifically for this study and is explained.

2.1. N-body model of asteroids

We model asteroids as a collection of hundreds to thousands of hard spherical particles that interact gravitationally and through collisions. We use the *N*-body code, `pkdgrav`, which is an hierarchical tree code based on a symplectic leapfrog integration routine and is parallelised. The tree allows for significant increases in the speed of integration, at the cost of small errors in force accuracy, making timestep selection important (smaller steps reduce the effect of the force errors, which tend to be randomly, not systematically, distributed). The code has been well-tested in a wide array of environments (see Richardson et al., 2002, 2009).

Within the integrator, collisions between particles are searched for with a tree: a configurable-number of nearest particles are checked for possible collisions during the next timestep. Multiple collisions among particles during the step are handled in time order. When two particles collide their resulting trajectories are determined using simple formulas for the rebound of two hard spheres. For impacts where the relative speed of the two particles is above 10% of their mutual escape speed (this percentage is a configurable parameter), the ratio of rebound speed to impact speed is controlled by the coefficient of restitution, typically around 0.5. Below 10% of their mutual escape speed, the collisions are perfectly elastic. Thus each rubble pile, represented by a group of self-gravitating hard spherical particles, is constantly in a state of low-energy excitement, with particles lightly bouncing off one another. The total vibrational energy, however, is always much less than the total self-gravitational energy of the rubble pile

The resolution, i.e. the number of particles constituting each rubble pile, has numbered between tens and thousands in previous simulations of the type presented here. The choice of resolution used in these kinds of studies of small asteroids is addressed in Walsh and Richardson (2006), where it is assumed that the fundamental building blocks constituting asteroids are ~150 m, and therefore a 1000-particle body would be ~3.3 km in diameter. This is the justification for using this particle size throughout, though we do present experimental results from simulations performed at higher resolution. Holsapple (2010) suggests that the resolution in our simulations, by way of creating "lumpiness", is an important factor for differences in results between the analytical continuum theory and *N*-body results. A larger investigation of shape change as a function of resolution is beyond the scope of this particular study, but may soon be practical with increases in computational speed.

2.2. Rubble piles – modeling different angle of friction

The behavior of the model rubble piles compared to known granular materials and analytical formalisms is important in interpreting the results of the experiments. The following sections detail our efforts to create a series of rubble piles that behave differently under the stresses of angular momentum changes and general rotational spin-up. The test used to estimate an angle of friction for each body is based on work by Richardson et al. (2005), where model rubble piles covering a wide parameter space of spin and shape were evolved and then compared to the analytical estimates of allowable spin and shape combinations computed in the continuum limit by Holsapple (2001, 2004). These tests do not provide a precise measure of the angle of friction, rather an estimate. Due to the fact that particles never rest on each other, and therefore have no surface friction to resist reshaping, we do not go further in estimating the precise granular properties of our simulations within the scope of this work. Rather we rely on the analytical results of Holsapple (2001, 2004) as a way of constraining the bulk behavior of our model rubble piles. We find, and will show in the following sections, that though our model rubble piles are essentially frictionless, they still in fact follow the limits derived by Holsapple when they are subject to angular momentum increase.

2.2.1. Model rubble pile creation

For our nominal case represented by a monodisperse population of particles (all particles having identical size and mass), each initial rubble pile is started in a close-packed formation. Variations of this scenario are used throughout this study, so the fundamental geometry is important to discuss. The theoretical maximum density for packing of spheres is attained with hexagonal closest packing (HCP), which results in a minimum void space of ~26% (see Leinhardt et al., 2000). When creating a rubble pile for simulations, the spheres are packed in HCP with 1% of the particle radius space between each particle. Each particle is then given a random

velocity vector with a magnitude of 1% of the particle's escape speed. The initial random energy minimizes numerical pathologies arising from simultaneous collisions and inelastic collapse (see Richardson et al., 2009) but is well below the energy required to re-shape the asteroid. Another benefit of this approach is that each generated rubble pile is slightly different, despite identical physical properties and initial packing configuration, as the initial particle velocities are random for each.

Variations on the nominal case of HCP are used for different initial rubble configurations, as not every rubble pile used in this work begins with a monodisperse population of particles. Most variations rely on using the original geometry of HCP, but with very large initial particle separations followed by a period of collapse, allowing for a random reconfiguration of the spheres. This method of rubble pile formation was used for all bi-modal particle distributions (two different particles sizes), and for placing surface particles around a large core.

For many simulations a rubble pile with an initial elongation was used as an initial condition. For all but the nominal case, where spheres can be packed into an ellipsoidal shape, the rubble piles were created by allowing a collapse of particles into a random configuration. In these collapse scenarios the bodies always end up nearly spherical. To create an elongated rubble pile for these cases it is necessary to initially create a large body with ~2000 particles. Then a routine is used to "carve" out an ellipsoid with the required shape, leaving ~1000 particles in an elongated and randomly configured rubble pile.

2.2.2. Nominal rubble pile

As described above, the nominal rubble piles in these simulations have identical spherical particles, in an initially excited hexagonal closest packing formation (HCP). For all simulations the particle density is 3.4 g cm^{-3}, and the bulk density for the nominal case was then ~2.3 g cm^{-3}. Simulations done by Richardson et al. (2005), using the same code, show that a monodisperse rubble pile behaves similarly to a cohesionless granular material with an angle of friction $\phi \sim 40°$.

These "re-shaping simulations" simply impart an initial spin on rubble piles of different initial elongations (ratio of the long axis to the short axis) and measure the resulting outcome (mass loss, reshaping, etc.). The final spin state and rubble pile shape/elongation are then compared to the classical fluid-equilibrium shapes, as well as the limits derived for cohesionless granular material (Holsapple, 2001, 2004). The angle of friction of dry sand is ~20°, whereas simple terrestrial material is expected to be around 30–40° (see Fig. 2 of Richardson et al., 2005).

2.2.3. The near-fluid case, $\phi \sim 0°$

A rubble pile that possesses near-fluid properties was created using a bi-modal particle size distribution. Using the rubble pile creation mechanism explained above, 33% of the ~1000 particles were randomly increased in size by 25% (their mass was also increased to keep particle density constant). The cloud of particles was then collapsed into a rubble pile that was randomly organized. The bulk density of the final rubble piles was ~2.0 g cm^{-3}.

The estimate of the angle of friction of this rubble pile was derived from a re-shaping simulation, similar to those performed for the nominal monodisperse case by Richardson et al. (2005). For the case of this bimodal rubble pile, regardless of its initial shape or spin, it quickly evolves to a nearly-fluid equilibrium state. The most dramatic examples of this behavior were cases of low spin-rate (9 h), and moderate elongation (a:c = 1.7:1). This shape/spin configuration is stable for even very modest angles of friction, but these rubble piles in the near-fluid case quickly evolved to a new state with a 7.75 h rotation period and an axis ratio of 1.5:1.14 (see Figs. 1 and 2).

2.2.4. Intermediate case

A rubble pile with the intermediate angle of friction was created using a bi-modal distribution of particle sizes, similar to the fluid model, but in this case 33% of the particles were made only 5% larger than the standard particle. Again, the rubble piles were created using a cloud of particles that was allowed to collapse under gravity, creating a random configuration of the particles with a final bulk density ~2.0 g cm^{-3}.

The re-shaping simulations performed on these rubble piles show behavior consistent with an angle of friction near ~20° (see Figs. 3 and 4). The piles starting with slow spins and moderate elongations were able to maintain their shapes. However the piles starting with elongation/spin configurations beyond the ~20° cohesion-less limit suffered shape changes. Those that started well beyond the ~20° cohesionless limit suffered major shape changes and evolved back to the classical fluid shapes. In short, these rubble piles re-shaped at spin rates intermediate to the fluid case and the nominal cases.

2.2.5. Rubble piles with cores

A final set of rubble piles tested had a core constructed of particles that were twice as large as the surrounding smaller particles. These core particles were placed in HCP formation, and a cloud of the smaller particles was then collapsed on top in a random configuration. Bodies with different sized cores were created, one each with 25%, 38% and 76% of the total mass in the core (Fig. 5). All bodies were used for some simulations, but only the bodies with 38% massive core were tested extensively. Since these rubble piles were not easily parameterized with an angle of friction (ϕ), the re-shaping simulations were not performed for them.

2.2.6. High resolution rubble piles

To check the simulations' sensitivity to component size, tests were run at varying resolution (different number of particles). At high resolution, due to the computational expense, only small subsets of the standard suite of simulations were carried out. Overall,

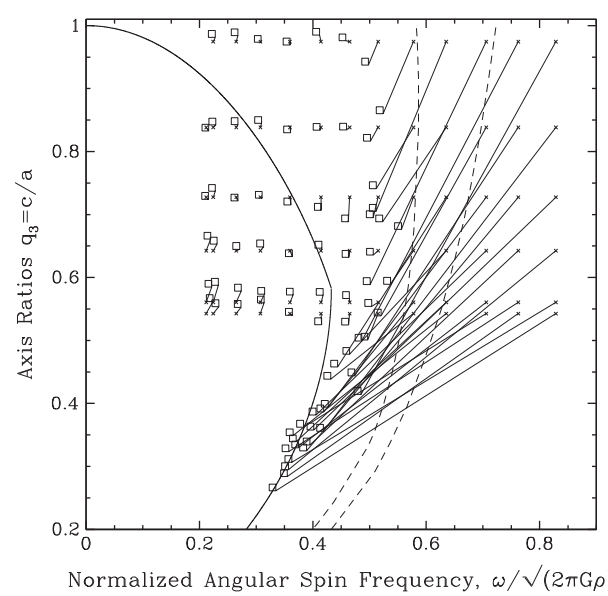

Fig. 3. The results of spin-limit tests for the "intermediate" rubble pile, created with a bi-modal size distribution of particles. The small crosses are the starting points of the rubble piles, and the lines connect to the open squares, which are located where rubble piles ended after evolving. The vertical axis is the c/a axis ratio of the rubble pile and it is plotted against the normalized angular spin frequency. The solid line is the Maclaurin/Jacobi fiducial for the c/a axis and the dashed lines are the analytical limits for the frictionless granular material with angles of friction of 20° (left) and 40° (right).

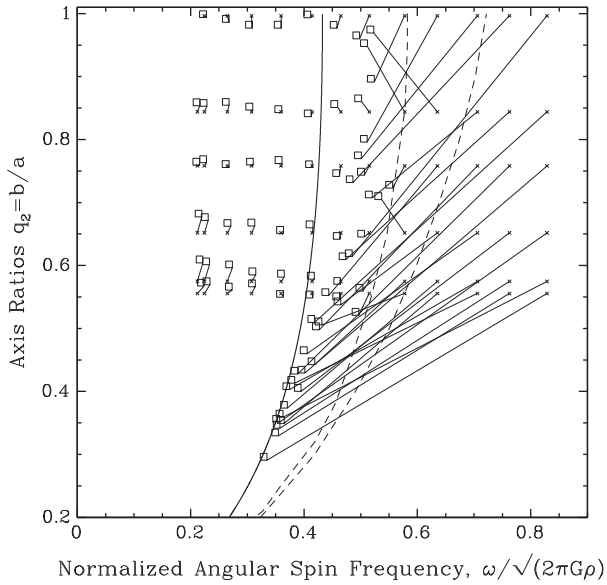

Fig. 4. The results of spin-limit tests for the "intermediate" rubble pile, created with a bi-modal size distribution of particles. The small crosses are the starting points of the rubble piles, and the lines connect to the open squares, which are located where the rubble piles ended after evolving. The vertical axis is the b/a axis ratio of the rubble pile and it is plotted against the normalized angular spin frequency. The solid line is the Maclaurin/Jacobi fiducial for the b/a axis and the dashed lines are the analytical limits for the frictionless granular material with angles of friction of 20° (left) and 40° (right).

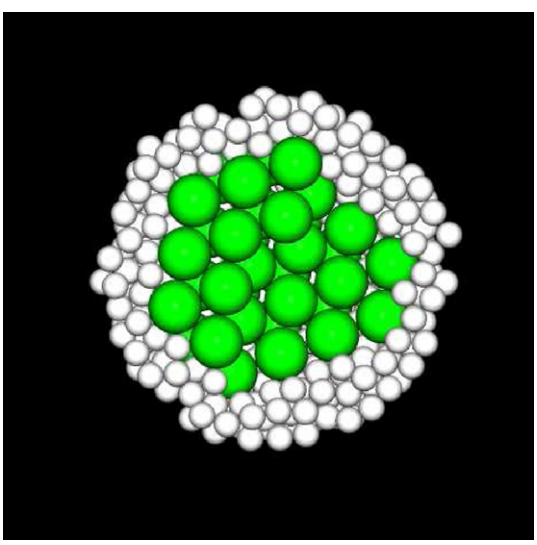

Fig. 5. Cross section of the large core model. The large, dark (or green) internal particles are in Hexagonal Close Packing formation, and quite rigid against re-shaping. The white, and smaller, surface particles are randomly oriented on top of the core. (For interpretation of the references to color in this figure legend, the reader is referred to the web version of this article.)

tests were run for cases ranging from 50 to 5000 particles. Results from these tests are discussed in Section 5.

2.3. Modeling spinup

The experiments call for a continuous and small increase of the body's angular momentum, affecting the entire body simultaneously, but not any ejected particles. For this model, angular momentum was increased in small discrete "boosts."

The two parameters governing the process are the time delay between spin boosts, and the magnitude of these boosts. After a series of tests to determine parameters that are both computationally expedient and which show a convergence in results, delays of 2000 timesteps (where each timestep was 50 s) and angular momentum increases of 1% were used. The delay of 2000 timesteps is roughly five spin periods, at the most rapid spin rates attained (~3 h). The boosts used were simply a 1% increase in the body's angular momentum.

Simulations were run varying the main spin-up parameters over an order of magnitude, namely the length of time between spin-boosts, and the magnitude of each spin-boost. Values of 200–20,000 timesteps were tested for the delay, and percentages from 0.1% to 2.5% were tested for spin-boost magnitude (see Figs. 6 and 7). It was determined that the standard values provide a spin-up that allows for the body to equilibrate in between spin increases, and is small enough to not initiate mass loss instantaneously, i.e., mass loss events and re-shaping occur equally spread throughout the simulation, and not directly following a spin increase.

Analysis of the velocity dispersion inside the rubble pile was done, searching for indication that any residual excitement caused by the angular momentum boost was settled. However, the excitement was so subtle, that the basic numerical excitation of the particles was greater than any excitement imparted during the spin-up procedure.

2.3.1. Basic integration parameters

The basic parameters governing the numerical integrations of the rubble piles are quite similar to those used in past simulations for tidal disruptions and rubble pile collisions (Walsh and Richardson, 2006, 2008; Leinhardt et al., 2000). The timestep for each simulation was 10^{-5} year/2π (~50 s), which is less than 2% of each particle's dynamical time. Simulations were run for 2×10^6 timesteps in most cases, and sometimes extended to 3×10^6 timesteps.

This overall simulation time is drastically shorter than a true YORP timescale, but due to the computational expense, a simulation at the correct physical timescale is impossible with current computing facilities. The spin increase is so small over the entire YORP timescale that artificially accelerating the spin-up process

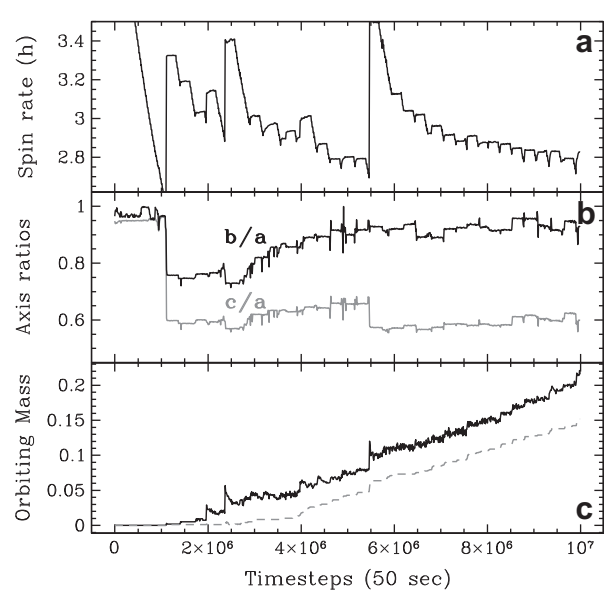

Fig. 6. Simulation using a 20,000 timestep delay between spin boosts. The resulting (a) spin rate, (b) axis ratios and, (c) mass loss and satellite accumulation plotted versus timesteps, can be compared against the results in Fig. 8.

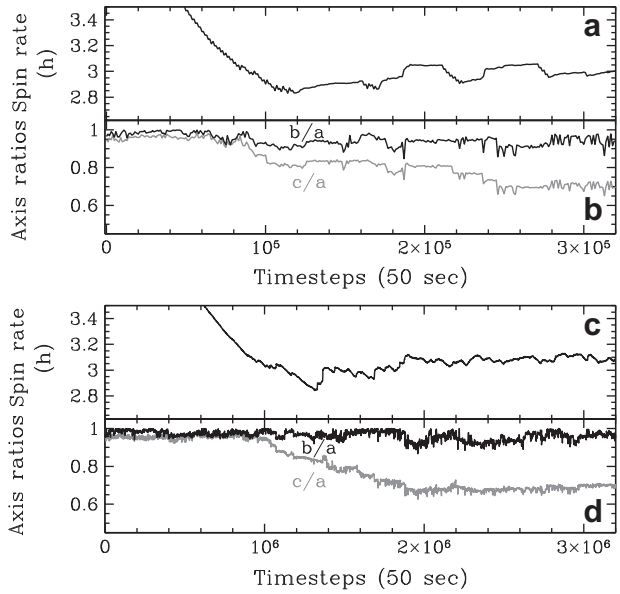

Fig. 7. Comparison of simulations using a 1% angular momentum boost (top two panels, a and b) with the nominal case of 0.1% (bottom two panels, c and d). The evolution of spin rate and spin axes are plotted against the timestep. Note that the bottom two panels cover 10 times more steps due to the factor of 10 in the amount of angular momentum imparted at each boost.

is unlikely to significantly affect the outcome of the re-shaping body (which our tests support). However, other processes affecting the accretion of the satellite could be more sensitive to shortened timescales – these are addressed more directly in Section 5.

The normal coefficient of restitution, the main parameter used to govern collisional outcomes between particles, was an important parameter in these simulations, which we varied between 0.2 and 0.8. The tangential coefficient of restitution is what would govern "sliding friction" and would allow angular momentum transfer from particle to particle. However, this is a poorly constrained parameter and somewhat artificial since real particles are not expected to be perfectly spherical. Therefore it was not varied among the tests and remained at unity, meaning no change in lateral motion (or spin) occurred as a result of collisions.

3. Analysis

3.1. Spin and shape changes

The spin and shape of the bodies (either the entire body, or the largest remnant after mass has been ejected), were monitored throughout each simulation. The shape was measured by fitting a tri-axial ellipsoid around the body and calculating the semi-axes of the fitted ellipsoid, *a*, *b* and *c* (from longest to shortest). The density of the body was calculated with the mass inside of this ellipsoid and the volume of the ellipsoid. Some shapes are better characterized with simple ellipsoids than others, and therefore this particular step of the analysis could introduce some small errors. Density, in particular, is sensitive to the volume analysis as it is used in the normalized spin frequency calculations, and any errors tend to underestimate bulk density.

For calculations involving the evolution of the "surface" of the asteroids, the particles initially on the surface of the model rubble pile are tracked throughout the simulations.

3.2. Orbit analysis for ejected material

In all simulations, the body was spun-up to the rotation rate at which particles were ejected from the surface. At this point in the simulation, the spin-up procedure only applies to the largest body, and additional analyses are made. The shape, spin and density of the main body and the largest orbiting mass are calculated, as well as the amount of mass ejected from the system, and the amount still bound to the main body. The orbital properties of the largest orbiting mass were analyzed using the program `companion` (Leinhardt and Richardson, 2005).

The final properties of the secondaries are a strong function of when the simulations are stopped or analyzed. The spin-up of the main body is artificially imposed and does not depend on the changing shape of the body, or the ejection of mass. However, among the observed population of NEA binaries, only one is known to have a secondary exceeding 50% the size of the primary (there is a subset of MBA binaries that appear to have near similar-sized components, see Behrend et al., 2006). So there is likely a mechanism that stops mass from being transferred to the secondary. The moment in time at which this happens is unclear, and therefore it is difficult to determine at what point the simulations should be compared with the actual observed binary population.

For consistency, we analyze secondaries when they have become 30% the size of the primary. This was based partly on work by Ćuk (2007), in which the Binary-YORP (BYORP) effect was estimated to dominate over the YORP effect when the satellite reached this size, halting mass transfer. The BYORP effect is a thermal effect similar to YORP that acts on a synchronized binary system rather than a single body; the secondary acts as a lever-arm for providing torques to the primary (note that there have been multiple works on BYORP following that of Ćuk, and they make a wide range of different predictions – most are beyond the scope of this work (McMahon and Scheeres, 2010a,; Steinberg and Sari, 2011; Jacobson and Scheeres, 2011b)). The YORP effect is dependent only on the size, shape and heliocentric orbit of the primary. The BYORP effect is more complex and depends on the relative sizes of the primary and secondary, their mutual orbit, and the spin states of both. One estimate derived when the BYORP effect becomes dominant finds that this occurs when the secondary is about 30% the size of the primary (Ćuk, 2007). This value is also very typical of the observed size of the secondary for this class of binary (between 20% and 50%), and therefore provides a good starting point for matching properties of binaries.

The shape of the secondary is not well-constrained in most simulations due to the small number of particles constituting those bodies when the simulations are analyzed (usually ~30). However, the spin rate and basic orbital properties of the satellites are robust.

3.3. Suite of simulations

For the nominal case of the monodisperse rubble pile, the differences between each rubble pile are strictly in the random velocities imparted on each particle, but for the other cases the actual configuration of particles in the initial rubble pile is different from one rubble pile to the other.

The nominal case was used for two initial shapes: spherical and prolate. The prolate body had axis ratios of 2:1:1, where the long axis, *a*, was twice as long as the intermediate, *b*, and short axis, *c*. For each shape, simulations were run with four different normal coefficients of restitution: 0.2, 0.4, 0.6 and 0.8. The initial spin rate for this nominal case is 4.4 h, which is within the spin limits for a cohesionless granular material with an angle of friction ~40°.

The other test cases involve the variant rubble pile structures described above: $\phi \sim 20°$ angle of friction (intermediate case), $\phi \sim 0°$ angle of friction (fluid-like case), and those with a rigid core consisting of 38% of the mass. Other parameters remained the same, except that for the fluid-like and intermediate cases the initial spin was 10.4 h, since a 4.4 h rotation would immediately

re-shape the bodies. For the simulations of rubble piles with cores, no prolate cases were tested.

For every simulation performed, data was output every 1000 timesteps, providing detailed temporal resolution of changes to the body or binary system. For each set of parameters (for example a spherical nominal rubble pile, coefficient of restitution of 0.2) ten simulations were run each using a unique progenitor. The results presented below focus on the physical changes to the body before and after mass ejection, as well as the properties of any orbiting body.

4. Results

Multiple simulations were run for each set of parameters but in the following, for the sake of brevity, we will often describe only a representative case when most simulations follow similar evolutionary paths. Nevertheless, many of the following plots and tables include results of the entire suite of simulations. The satellite properties are briefly discussed in the sections describing the different types of rubble piles used, though Section 4.5 at the end discusses all of the satellites and compares them with the known population of binary asteroids.

4.1. Nominal case

4.1.1. Shape and spin changes

In tests with initially spherical bodies, the first shape change begins at a spin rate of 2.9 h (see Fig. 8). The body spins to its minimum spin rate at ~2.8 h, at which time more re-shaping and the first mass loss occurs, pushing the axis ratio c/a to ~0.8, while b/a stays near unity for the entire simulation. This re-shaping, where the c/a axis ratios adjust, is the start of the transition from spherical to oblate. The long and intermediate axes, a and b, remain nearly equal, while the short axis becomes significantly shorter than both. The next major re-shaping occurs after continued mass loss pushes the c/a value to ~0.65, where it stays for the rest of the simulation (see Figs. 9 and 10). At these axis ratios the body maintains a spin rate ~2.9–3.1 h, and loses mass steadily without more dramatic reshaping.

Fig. 9 shows the evolution of a body, and shows the body is able to hold an equilibrium shape well beyond the fluid limit, as observed by Richardson et al. (2005). Fig. 10 shows the end-of-simulation average axis ratios for the different types of rubble pile tested, with the nominal case having average $c/a = 0.70$ and $b/a = 0.90$.

Results for initially prolate bodies were quite similar, though the body first shed mass from the ends of its long axis, before commencing the behavior described above. After significant mass was lost from the long ends of the body it then largely converged onto the behavior found for the initially spherical bodies. High-resolution versions of the spherical, nominal, 0.2 coefficient of restitution runs were carried out. In general we found little change to our results compared to the 2000 particle tests, and some slight divergences with the 5000 particle test which are discussed later (see Figs. 18 and 19).

4.1.2. Mass loss and satellite formation

As noted above, mass loss begins soon after the body becomes slightly oblate (shown in Fig. 8 at timestep 1.2×10^5, and by the black square in Fig. 9). The first mass that is ejected comes from the equator (see Fig. 11). Mass loss following this event continues from similar areas near the equator. The ejected mass accumulates into a satellite for some of the tested properties with this nominal case, and is strongly dependent on the coefficient of restitution of the material in the simulation. For the lowest value of coefficient of restitution tested, 0.2, satellite accumulation is efficient with nearly 50% on average of the ejected mass being accumulated into the satellite (see Table 1). Higher values of coefficient of restitution proved less efficient at forming satellites, and for values above 0.6, no satellite formation occured.

4.1.3. Satellite properties

When satellite formation occurs, the systems initially have very small semi-major axes, typically $a \sim 2.5$–3.5 primary radii (R_{pri}; see

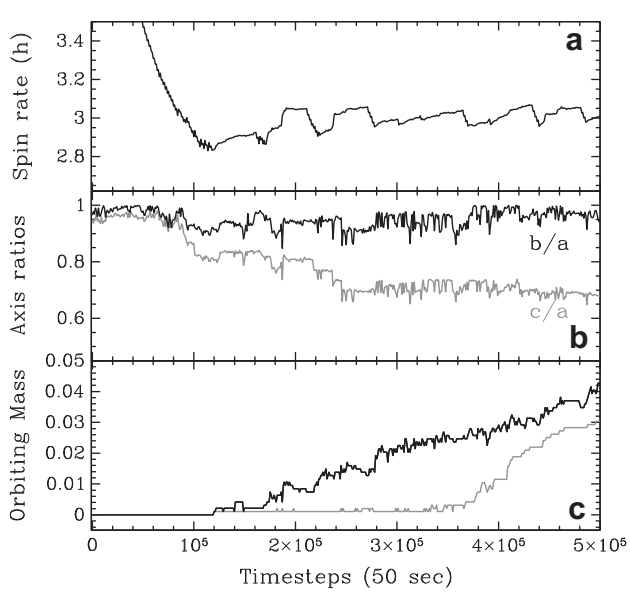

Fig. 8. The early stages of mass loss, re-shaping and binary formation for a nominal test (the first listed in Table 1). The top frame (a) shows the evolution of the spin rate of the primary body during the first 5×10^4 timesteps. Frame (b) shows the evolution of the axis ratios, b/a and c/a over this time interval, and the bottom frame (c) shows the fraction of orbiting mass (dark line) and the size of the largest satellite (gray line).

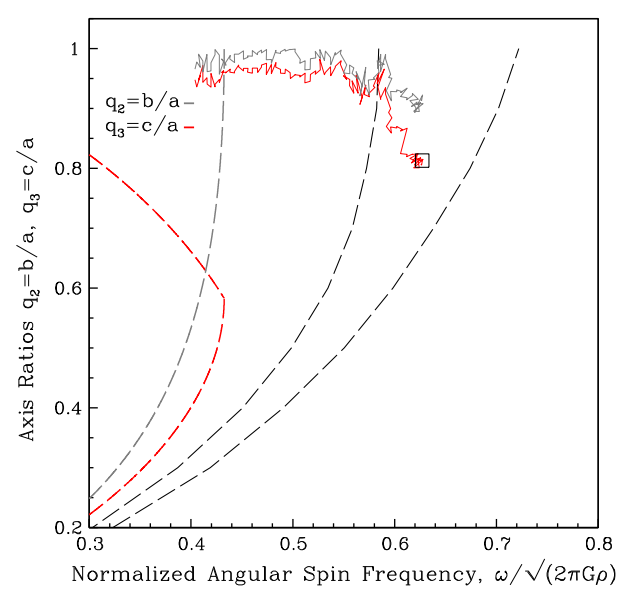

Fig. 9. The evolution of the axis ratios is shown by the solid lines plotted as a function of the normalized angular spin frequency. The first moment of mass loss is indicated by the black square. The thin red and gray lines track the spin axes of the main body, c/a and b/a respectively, and show how the shape of the body goes beyond the analytical predicted limits for a granular material with 20° angle of friction (2nd from the right dashed line), and nearly to the 40° limits (rightmost dashed line). (For interpretation of the references to color in this figure legend, the reader is referred to the web version of this article.)

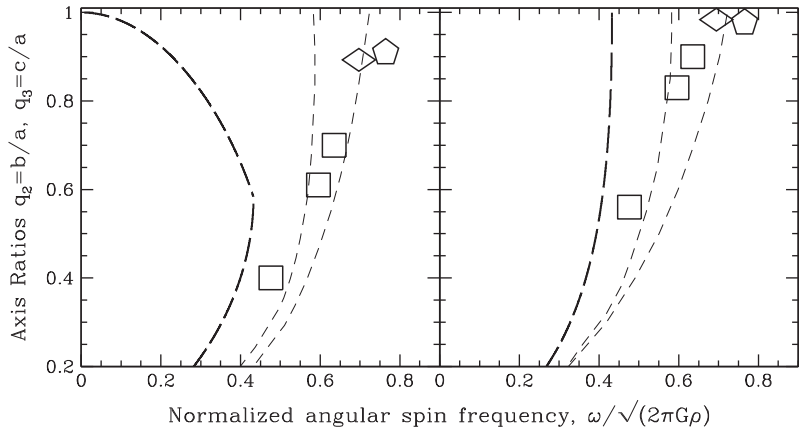

Fig. 10. The average axis ratios for each of the three rubble pile types as a function of the normalized angular spin frequency. The left panel is the c/a axis ratios of (top) nominal, (middle) intermediate and (bottom) fluid rubble piles. The thick line is the Jacobi/Maclaurin limit and the dashed lines are the analytical estimates for 20° and 40° angle of friction. The right panel is the b/a axis ratio and with the same fiducials. Also plotted are the properties for the two best studied primaryies from NEA binary systems; 1999 KW_4 (diamond shape) and 1994 CC (pentagon shape) (Ostro et al., 2006; Brozović et al., 2011).

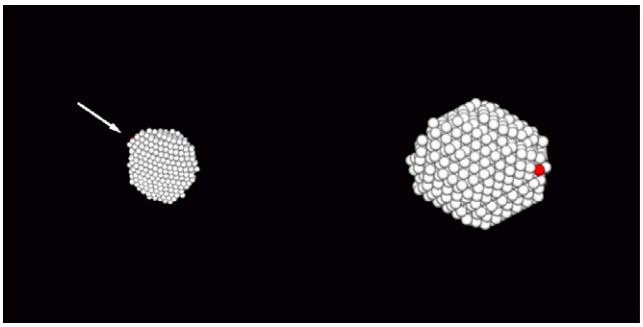

Fig. 11. Left: a nominal body as viewed looking down its rotation axis at the time of first mass loss. The red particle in the upper left, on the equator, is the first particle lost. Right: the same body but viewed looking at the equator, with the spin axis pointing up. Again, the red particle is the first ejected. (For interpretation of the references to color in this figure legend, the reader is referred to the web version of this article.)

Table 1). For components of similar density, the Roche limit is $2.46R_{pri}$, signifying that initial accumulation of a satellite is likely to happen just outside the limit (see Fig. 12). In a handful of cases, the initial a/R_{pri} is less than 2.46, suggesting that variations in the system, secondary rotation rate and/or density allow for satellite accumulation at a smaller semi-major axis. The eccentricities were typically below 0.2, and were frequently below 0.05.

After only a few particles have accumulated most of the remaining orbiting debris is quickly accreted (as seen in Fig. 8, where ~2.5% of the mass is in orbit before the first large satellite forms, and then it accumulates nearly all the orbiting mass quickly). Satellite formation then continues with high efficiency until the mass of the secondary nears the mass of the primary ($M_{sec} > 0.5M_{pri}$), at which point our simplified model of YORP breaks down as we model a generic spin-up much faster than tidal forces or other radiation forces could operate (we measure satellite properties at $R_{sec} \geqslant 0.3R_{pri}$, where R_{sec} is the secondary radius; see Section 3.2).

The material that forms the secondary originates primarily on the surface of the progenitor asteroid. To study surface material transfer, we color-coded original surface particles in our nominal, low coefficient of restitution simulations (see Fig. 1 of Walsh et al., 2008). The results show that 70–90% of the particles in the secondary were originally surface particles on the primary. Also, 15–35% of the surface of the primary at the end of the simulations are uncovered particles that did not originate at the surface.

4.2. Intermediate case

The intermediate case was designed to have properties placing it somewhere between the nominal case and the fluid case. This allowed the bodies to deviate from the fluid limits and maintain less elongated shapes at critical spin rates and mass loss. The evolution of these rubble piles shows that the piles are indeed an intermediate case, as they do not immediately re-shape to fluid shapes. However, as the simulations progress, and the body is pushed to more rapid spin rates, the body re-shapes and loses mass beyond the fluid limits, but before they reach the 20° angle of friction limits. The first mass loss occurs just as the c/a axis ratio reaches the 20° limit. At this point the axis ratios are $b/a \sim 0.8$ and $c/a \sim 0.45$. As the simulation progresses, the body does not continue to get more elongated, and instead maintains a roughly constant shape (see Fig. 13). The average axis ratios for the length of the simulation stay very near those at which first mass loss occurs, with average end-of-simulation ratios of $c/a \sim 0.61$ and $b/a \sim 0.83$ (see Fig. 10).

4.2.1. Mass loss and binary formation

The first mass loss does not occur until after significant re-shaping and the body has achieved its most elongated axis ratios, approximately 1:0.8:0.4. This happens near timestep 300,000 (recall, timesteps are ~50 s), after gradual reshaping began at timestep 100,000 (see Fig. 11). The spin period at this first mass loss is ~3.5 h.

The satellite accumulation is delayed until ~7% of the total system mass is in orbit around the primary body. In the nominal case, once the satellite formation begins, the secondary rapidly gains mass, efficiently accumulating ejected material.

The intermediate case was not always favorable for satellite formation, and in many cases did not form any satellites. The maximum equatorial elongations attained in these cases, $c/a \sim 0.40$, are less extreme than for the following fluid cases, but much more extreme than the nearly spherical/oblate shapes created in the nominal case. These intermediate cases indicate a limiting equatorial elongation required for satellite accumulation, where elongations less than $b/a \sim 0.8$ (more elongated) stifle satellite accumulation. The presumed mechanism at play here is increased relative velocities between particles due to orbital excitement by the nearby irregularly shaped primary. Lightcurve observations of known NEA binary systems find primaries with lightcurve amplitudes less than 0.2 mag, which translates to $b/a \sim 0.8$ (Pravec

Table 1
Tabulation of satellite properties.

Initial elongation	Rubble pile type	ϵ_N	M_{sec}/M_{pri}	a/R_{pri}	e	Time steps (50 s)	a/b	a/c	Orbital period (h)	Secondary rotation (h)
1	Nominal	0.2	0.027	2.545	0.165	452,000	1.03	1.46	14.296	6.58222
1	Nominal	0.2	0.028	2.562	0.088	504,000	1.04	1.37	13.294	11.7979
1	Nominal	0.2	0.027	2.816	0.053	424,000	1.16	1.46	16.713	7.81839
1	Nominal	0.2	0.029	2.255	0.031	447,000	1.01	1.39	11.67	6.95934
1	Nominal	0.2	0.027	3.408	0.203	383,000	1.11	1.47	21.273	12.9674
1	Nominal	0.2	0.029	3.552	0.042	1,731,000	1.02	1.62	23.246	7.03076
1	Nominal	0.2	0.027	2.687	0.120	499,000	1.03	1.41	14.304	10.1341
1	Nominal	0.2	0.028	2.434	0.107	532,000	1.00	1.41	13.612	8.42117
1	Nominal	0.2	0.027	2.718	0.148	939,000	1.11	1.49	14.862	11.8793
1	Nominal	0.2	0.027	3.426	0.113	441,000	1.07	1.47	22.128	5.78855
1	Nominal	0.4	0.027	2.883	0.093	414,000	1.12	1.45	17.011	7.54632
1	Nominal	0.4	0.027	2.501	0.142	621,000	1.02	1.38	13.285	7.97188
1	Nominal	0.4	0.028	3.179	0.087	770,000	1.08	1.44	19.537	12.225
1	Nominal	0.4	0.028	3.645	0.164	426,000	1.05	1.48	22.938	8.42375
1	Nominal	0.4	0.029	2.469	0.113	764,000	1.05	1.49	14.016	6.2652
1	Nominal	0.4	0.028	2.320	0.066	412,000	1.08	1.44	11.882	10.6458
1	Nominal	0.4	0.027	2.872	0.266	669,000	1.02	1.48	15.874	5.92096
1	Nominal	0.4	0.030	2.236	0.057	441,000	1.08	1.47	11.496	6.50503
1	Nominal	0.4	0.027	3.100	0.114	632,000	1.03	1.49	11.796	9.95245
1	Nominal	0.6	0.028	3.480	0.095	777,000	1.09	1.60	19.514	5.49011
1	Nominal	0.6	0.033	3.042	0.110	1,107,000	1.02	1.47	23.033	25.2806
1	Nominal	0.6	0.028	2.715	0.055	561,000	1.04	1.57	18.271	8.47915
1	Nominal	0.6	0.028	2.354	0.047	515,000	1.05	1.54	15.869	9.95821
1	Nominal	0.6	0.027	2.868	0.038	648,000	1.04	1.51	12.136	7.58112
1	Nominal	0.6	0.028	3.409	0.067	1,182,000	1.08	1.56	17.367	6.14368
1	Nominal	0.6	0.028	2.139	0.107	1,492,000	1.09	1.62	23.047	5.6183
1	Nominal	0.6	0.028	3.540	0.236	830,000	1.07	1.53	24.461	8.05889
1	Nominal	0.6	0.027	3.367	0.164	901,000	1.13	1.64	22.276	8.39984
1	Nominal	0.6	0.028	2.876	0.243	822,000	1.03	1.47	16.678	9.90105
2	Nominal	0.2	0.028	2.287	0.089	1,907,000	1.18	1.41	11.989	7.5289
2	Nominal	0.2	0.028	2.288	0.044	2,106,000	1.09	1.35	11.108	6.75793
2	Nominal	0.2	0.028	2.962	0.055	1,914,000	1.21	1.47	16.879	7.75681
2	Nominal	0.2	0.028	2.289	0.151	2,080,000	1.07	1.35	10.796	6.36716
2	Nominal	0.2	0.028	3.087	0.101	2,331,000	1.04	1.32	16.438	7.53739
2	Nominal	0.2	0.028	2.355	0.083	2,499,000	1.16	1.66	13.091	6.15114
2	Nominal	0.2	0.027	2.406	0.077	2,183,000	1.05	1.38	12.043	9.4678
2	Nominal	0.2	0.027	2.702	0.068	2,109,000	1.27	1.44	15.345	7.40319
2	Nominal	0.2	0.028	3.707	0.052	2,765,000	1.10	1.43	23.731	35.2102
2	Nominal	0.2	0.028	2.646	0.126	2,096,000	1.15	1.38	13.013	6.67218
2	Nominal	0.4	0.028	3.897	0.291	2,466,000	1.09	1.37	24.492	5.29302
2	Nominal	0.4	0.027	2.090	0.151	2,123,000	1.12	1.52	10.809	5.60126
2	Nominal	0.4	0.028	2.852	0.069	2,288,000	1.19	1.45	15.919	5.69843
2	Nominal	0.4	0.030	3.093	0.083	2,664,000	1.02	1.40	17.874	8.39332
2	Nominal	0.4	0.027	2.081	0.025	2,116,000	1.10	1.36	9.576	5.65581
2	Nominal	0.4	0.027	2.860	0.167	2,047,000	1.14	1.40	15.99	8.2868
2	Nominal	0.4	0.028	2.576	0.034	2,152,000	1.03	1.33	12.856	7.6194
2	Nominal	0.4	0.028	2.668	0.185	2,407,000	1.05	1.32	13.697	5.16987
2	Nominal	0.4	0.028	3.133	0.033	2,327,000	1.07	1.44	18.776	11.5001
2	Nominal	0.6	0.025	3.403	0.124	3,000,000	1.03	1.20	18.966	9.7401
2	Nominal	0.6	0.027	3.116	0.065	2,657,000	1.04	1.44	18.946	4.0116
2	Nominal	0.6	0.027	2.437	0.150	2,587,000	1.12	1.42	12.818	9.19996
1	Intermediate	0.2	0.029	2.429	0.079	1,209,000	1.050	1.933	15.523	7.53874
1	Intermediate	0.2	0.028	2.905	0.083	836,000	1.095	1.653	17.42	6.94089
1	Intermediate	0.2	0.027	3.093	0.183	1,383,000	1.026	1.630	19.695	6.5501
1	Intermediate	0.2	0.028	2.127	0.051	1,120,000	1.018	1.591	10.809	7.05634
1	Intermediate	0.2	0.028	2.091	0.114	1,870,000	1.108	1.907	13.827	6.86763
1	Intermediate	0.2	0.028	3.034	0.213	587,000	1.010	1.561	19.4	7.89222
1	Intermediate	0.2	0.028	2.729	0.168	1,110,000	1.011	1.530	16.529	15.4522
1	Intermediate	0.2	0.028	2.272	0.077	551,000	1.059	1.635	11.507	7.80682
1	Intermediate	0.2	0.029	2.708	0.222	986,000	1.001	1.597	16.782	6.69458
1	Intermediate	0.2	0.028	3.696	0.252	1,011,000	1.004	1.499	26.244	5.38413
1	Intermediate	0.4	0.029	3.214	0.114	1,115,000	1.058	1.584	21.513	9.60038
1	Intermediate	0.4	0.028	3.232	0.183	1,066,000	1.001	1.533	20.953	6.49128
1	Intermediate	0.4	0.027	2.137	0.077	1,316,000	1.076	1.624	11.549	14.7263
1	Intermediate	0.4	0.028	3.654	0.095	1,648,000	1.052	1.643	24.875	6.54447
1	Intermediate	0.4	0.027	3.102	0.145	617,000	1.010	1.716	21.665	9.00378
1	Intermediate	0.4	0.027	2.743	0.102	1,064,000	1.017	1.599	16.356	6.03855
1	Intermediate	0.4	0.029	3.103	0.078	906,000	1.015	1.567	20.055	9.9363
1	Intermediate	0.4	0.028	4.192	0.187	1,045,000	1.011	1.573	29.985	8.38712
1	Intermediate	0.6	0.027	4.027	0.092	1,288,000	1.003	1.517	30.7	13.9623
1	Intermediate	0.6	0.028	3.411	0.074	1,223,000	1.014	1.550	24.446	4.75037
1	Intermediate	0.6	0.027	3.205	0.027	1,795,000	1.031	1.559	20.76	6.22388
1	Intermediate	0.6	0.027	2.751	0.147	1,966,000	1.091	1.595	18.298	8.70014
1	Intermediate	0.6	0.028	2.378	0.044	1,132,000	1.078	1.496	13.347	12.9629

Table 1 (*continued*)

Initial elongation	Rubble pile type	ϵ_N	M_{sec}/M_{pri}	a/R_{pri}	e	Time steps (50 s)	a/b	a/c	Orbital period (h)	Secondary rotation (h)
1	Intermediate	0.6	0.027	3.539	0.061	1,406,000	1.077	1.625	24.179	12.7932
1	Intermediate	0.6	0.028	2.239	0.171	1,434,000	1.011	1.615	12.113	11.8858
1	Intermediate	0.6	0.028	2.711	0.098	1,482,000	1.090	1.575	17.056	17.5388
2	Intermediate	0.2	0.029	2.848	0.155	1,755,000	1.007	1.525	18.047	7.44478
2	Intermediate	0.2	0.027	3.414	0.203	1,656,000	1.326	1.737	29.018	6.12714
2	Intermediate	0.4	0.028	3.305	0.136	1,965,000	1.159	1.770	24.845	6.89447
1	Core	0.2	0.027	2.212	0.131	701,000	1.202	1.890	13.753	9.11466
1	Core	0.2	0.027	2.797	0.100	1,674,000	1.245	1.371	16.425	8.76895
1	Core	0.2	0.025	2.133	0.032	2,000,000	1.320	1.432	11.256	6.11021
1	Core	0.2	0.027	2.506	0.021	763,000	1.274	1.310	15.063	15.0863
1	Core	0.2	0.027	2.389	0.028	1,740,000	1.161	1.410	12.591	9.16888
1	Core	0.2	0.027	2.344	0.067	1,400,000	1.269	1.365	13.119	11.3612
1	Core	0.2	0.023	2.662	0.025	2,000,000	1.218	1.353	14.375	8.96998

Summary of the parameters and properties for all binaries formed in the suite of simulations. The angle of friction, ϕ, is used to denote the type of progenitor in each simulation, ϵ_N is the coefficient of restitution, M_{sec}/M_{pri} is the mass of the secondary when the binary properties were analyzed, a/R_{pri} is the semi-major axis of the secondary in terms of the primary radii, e is the eccentricity of the system, *timesteps* is the number of 50 s timesteps it took to reach the critical secondary mass. The final axis ratios are listed, both b/a and c/a.

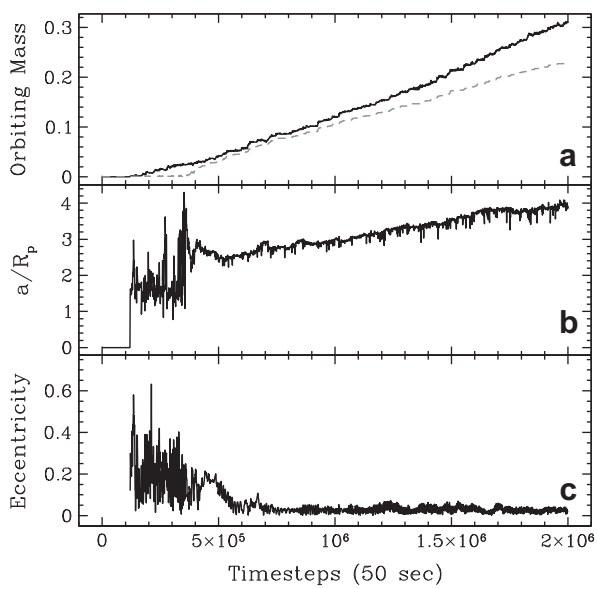

Fig. 12. The formation and evolution of a binary in the first nominal run, (a) total orbiting mass shown by the solid black line and mass in the largest satellite shown by the gray dashed line; (b) semi-major axis of the largest satellite in units of the primary radius; and (c) eccentricity of the largest satellite.

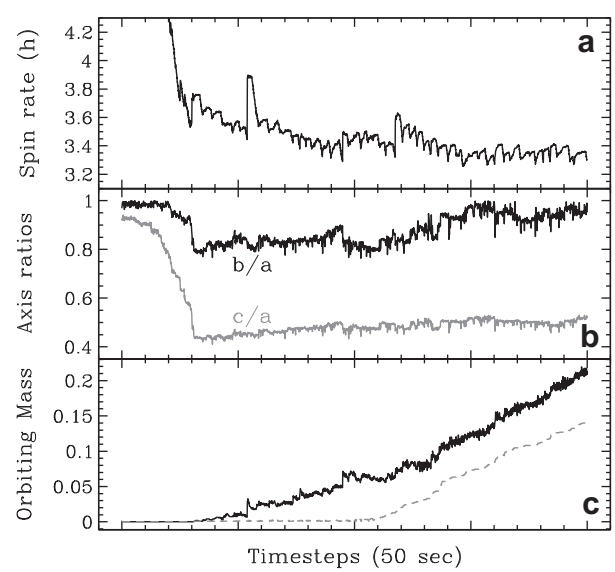

Fig. 13. Intermediate rubble pile simulation: (a) spin rate, (b) axis ratios; and (c) orbiting mass (dark solid line) and mass of largest satellite (gray dashed line).

et al., 2006). Of course equatorial asymmetries will not just affect the accumulation of a satellite in orbit, but also the long-term dynamics of any satellite that is able to form.

4.3. Fluid case

The fluid case never ventures far from classic fluid equilibrium shapes. At the outset of the simulation the body adjusts to a shape and spin state near the fluid equilibrium. Analytical descriptions of a classical fluid, with the initial spin of 10.4 h, suggest that neither a spherical nor a prolate shape with $c/a \sim b/a \sim 0.5$ is stable. As the spin is increased, the body continues to move to the right on the plot (see Fig. 10), reaching the position of maximum spin frequency for a fluid, near the bifurcation point where a Maclaurin ellipsoid goes tri-axial and becomes a Jacobi ellipsoid.

The average shape and spin rate that the fluid-like body maintains for the bulk of each simulation is a tri-axial ellipsoid with axes of roughly $b/a \sim 0.65$, $c/a \sim 0.4$ and a rotation period of 4 h (see Fig. 14). This configuration is very close to the Jacobi ellipsoid for a body with bulk density of 2.0 g cm^{-3} (see Fig. 10).

4.3.1. Mass loss and satellite formation

Mass loss begins after major re-shaping has occurred. The mass loss proceeds generally in the manner of single particles released from the end of the long axis of the near-equilibrium triaxial shape it attains. This triaxial shape frustrates satellite accretion for all values of coefficient of restitution tested. The body typically has an equatorial elongation of 2.5 (see Fig. 10), which causes significant perturbations for close-orbiting debris. Only a few fluid-like cases were observed to lose a significant number of particles at a given time (or between outputs); these are discussed in Section 4.6.

4.4. Rubble piles with cores

The evolution of the large-core models (38% of mass in core) progressed in a manner similar to the intermediate case. The axis ratios evolved with the body staying oblate (so b/a stayed constant, while c/a got smaller) up through the first instance of mass loss (Fig. 15). After the initial mass loss, the shape evolved slightly to attain average axis ratios of roughly 1.0:0.85:0.5. Despite the fluid-like flow of the exterior particles, the large cores restricted the overall elongation the body could attain. The cases with

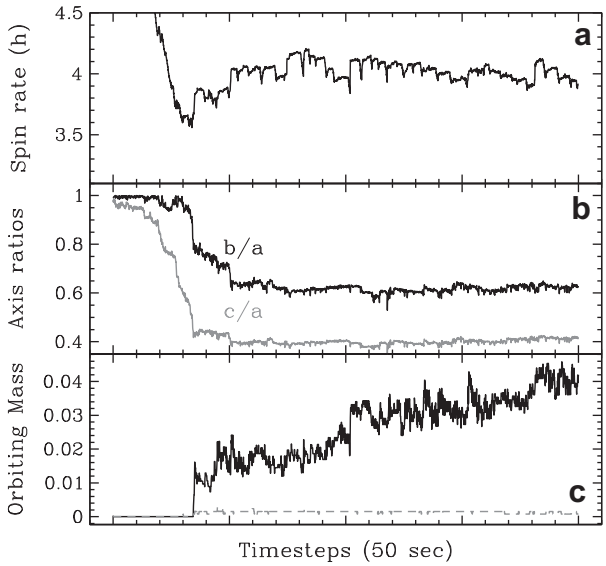

Fig. 14. Fluid rubble pile simulation: (a) spin rate, (b) axis ratios; and (c) orbiting mass (dark solid line) and mass of largest satellite (gray dashed line).

smaller cores behaved in a nearly fluid-like manner; in these cases the cores are insufficient to prevent the extreme axis ratios which are found in the fluid cases.

4.4.1. Mass loss and satellite formation

The relationship between equatorial elongation and successful satellite formation is again critical, and the small-core simulations flow in a fluid-like manner to take very elongated shapes. The large-core simulations produce satellites due to the relatively moderate maximum elongations, which rarely exceed ratios of a/b more extreme than 1:0.8.

4.5. Summary of satellite formation

In nominal simulations with initially spherical shapes the satellites typically accumulate around timestep 500,000. In the cases where satellites form, at the time the satellites reach the 30% size threshold, they account for 39% of all mass ejected from the main body. It was common for the satellite to account for 50% or more of the total ejected mass. The results are different when starting with a prolate body, as satellite accumulation does not start until the main body is near spherical, and significant mass loss (from the system as a whole) occurs before that state is reached.

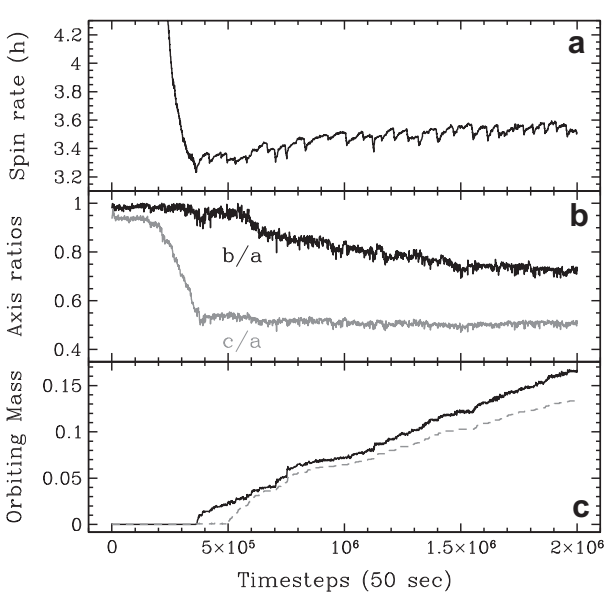

Fig. 15. The properties of the 38% core simulation, (a) the spin rate, (b) axis ratios and (c) orbiting mass the dark solid line and the mass of the largest satellite as the gray dashed line all plotted as a function of timesteps (50 s).

The satellites created in the nominal case are quite similar to the observed population of NEA binaries (Fig. 16). The secondaries formed in all the simulations have very low eccentricity, below 0.3 in all cases, where the average for the low coefficient of restitution nominal case is 0.1. Precise eccentricity measurements of observed NEA binaries are quite difficult to make, but the few solid measurements typically find values below 0.1 (Pravec et al., 2006). The satellites in the simulations reach critical size with very close orbits typically between 2.0 and $4.2R_{pri}$. The observed population of NEA binaries are typically found with very close orbits of 2.5–$5.5R_{pri}$.

The shape of the primary for observed binary systems is either based on shape models from radar observations, or estimated from lightcurve observations. Binaries discovered via lightcurve typically provide good constraints on the ratio of a/b for the primary body through the lightcurve amplitude. This ratio describes the elongation of the body's equator, or whether it is prolate, but it does not inform the observer about whether it is substantially oblate (as measured in a/c). A simple comparison of the observed systems and those from these numerical experiments find the population inhabiting the same range of $a/b = 1.0$–1.3 (Fig. 16). Bodies with irregular shapes, and very non-circular equators (a/b much greater than 1; meaning that they are prolate), would not be expected to survive in a stable dynamical configuration for long timescales (Scheeres, 2007). However, some of the observed oblate shapes may also be a natural outcome of a generic formation mechanism, as explored in this work (see Fig. 17).

4.6. Summary of mass shedding bursts

In a small number of simulations, limited to the fluid and intermediate cases, there was near-instantaneous, and significant, mass loss. For the sake of this investigation, we define a "mass shedding

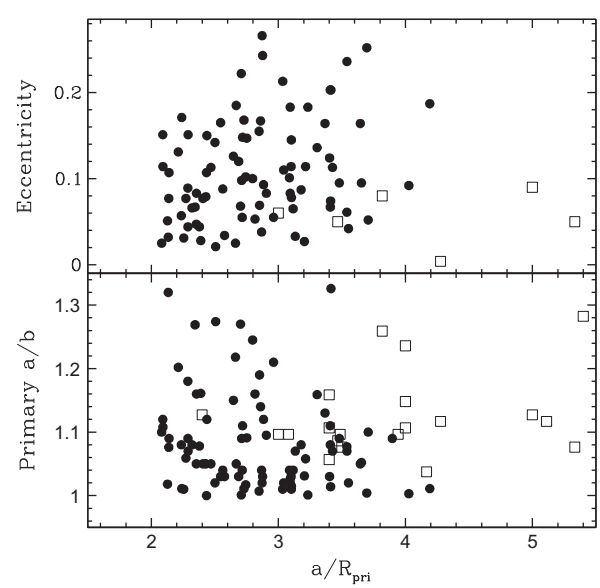

Fig. 16. Top panel: eccentricities of the secondary orbits from the simulations (solid circles) and the values measured or estimated for NEA binary systems (open squares) plotted as a function of their orbital semi-major axes. Bottom panel: primary axis ratio a/b for the binary systems created in the simulations (solid circles) and the values for known binary NEA systems (open squares) estimated by interpreting their lightcurve amplitudes ($\Delta m = 2.5\log(a/b)$), plotted against their orbital semi-major axes (Pravec et al., 2006; Harris, 2008 and references therein).

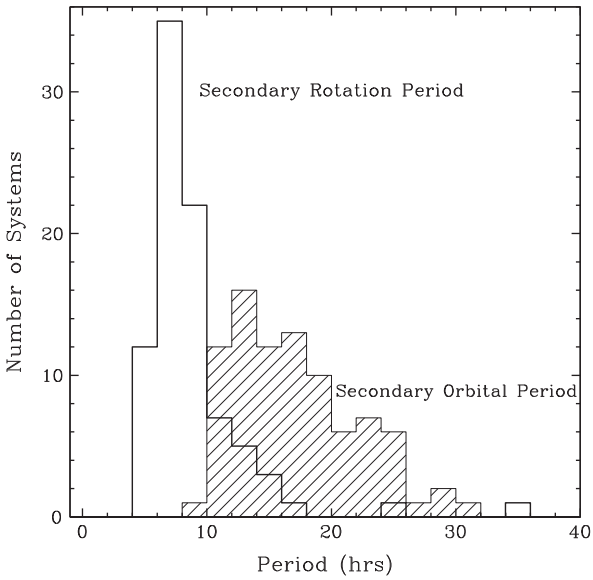

Fig. 17. Open histogram are the spin periods for all secondaries when they reach the critical size limit, and the hashed histogram shows the orbital periods for the secondaries at the same time.

burst" by a minimum mass loss of 2% of the primary in a single event. There were no simulations where a perfect or nearly perfect 50/50 split of the progenitor (a "fission" event) was observed – 7% was the maximum observed. Since normally we only output once every 1000 steps, a few cases where mass shedding bursts occurred were re-run with more frequent outputs. This often revealed the burst to in fact be a series of small mass losses, rather than an instantaneous loss of significant mass. All of the cases of 2% mass loss in an interval of 1000 timesteps (about 14 h) were considered substantial and all cases are listed in Table 2.

The rubble pile was always of fluid-like or intermediate nature, and had evolved into a prolate ellipsoid. The bursts occured between spin periods 3.1–5.1 h, with elongations (long over short axes) of 1.4–2.9. In sum these occured in only 29 cases with 9 having multiple occurrences of "mass shedding bursts" in a single set of parameters. Most cases barely achieved the 2% threshold, with only 2 shedding more than 5% of their mass in the 1000 timestep time interval, out of a total of 360 total simulations.

The progenitors in the simulations were all spherical or ellipsoidal shapes with variations from perfectly smooth shapes typically just a function of the radii of each discrete particle. The simulations never evolved into a bi-modal mass distribution, or had any irregular mass distributions (e.g., Itokawa). Investigation of separation of large components of a granular body from a bi-modal or contact-binary state will be left for future studies.

5. Discussion and conclusions

The main conclusions from these experiments of gradual angular momentum increase of a rubble pile asteroid are the following:

- Simple numerical models of rubble pile asteroids can be related to actual granular material through "re-shaping simulations" that match their re-shaping behavior to Mohr–Coulomb analytical formalisms. Those bodies with the highest estimated angle of friction, $\approx 40°$, maintain oblate shapes while reaching critical rotation, matching an observed property of many small asteroids with satellites.
- In the nominal tests, i.e. those with the largest angle of friction ($\phi \sim 40°$), mass loss occurs at or near the equator of the rapidly rotating body. As the body re-shapes and evolves, mass flows to the equator and is ejected into orbit. Bodies that are initially prolate lose mass from the ends of the long axis until they are nearly spherical, at which time they take and keep a spherical/oblate shape.
- Satellite formation by slow spin-up depends on the asteroid's ability to maintain low equatorial elongation, and for the asteroidal material to dissipate energy during collisions. The cases where large satellites formed were for the nominal and large-core tests with coefficients of restitution below 0.6. The intermediate cases also formed satellites, though with less efficiency than the nominal or core cases. The fluid-like cases never led to significant satellite accretion.
- The bodies that formed satellites due to slow spin-up (our proxy for the YORP-effect), had a significant portion of their surface removed and had subsurface material uncovered. In these simulations, the poles are where material was first uncovered, and much of the displaced surface material constitutes the satellite. This scenario is currently unique to this model of binary formation, and could be observable with thermal or radar observations. Recent thermal-IR observations currently support this hypothesis, as NEAs with satellites have been observed to have different thermal properties, cooler surface temperatures, than NEAs without satellites. These lower surface temperatures have been interpreted as a lack of regolith compared to NEAs without satellites Delbo et al. (2011).

Potential limitations in this study relate to modeling asteroids as collections of perfect spheres and the need to dramatically shorten timescales in the simulations. An actual asteroid, kilometers in diameter, will have a more complicated internal structure and therefore a potentially different response to angular momentum changes controlled by both the gravity and interlocking of its irregularly-shaped constituent pieces. Simulations are currently limited to modeling with perfect spheres, where the angle of friction is a function of particle interlocking and geometry. However, as mentioned above, our results show that only our model asteroids with the highest angle of friction can maintain oblate shapes at critical rotation rates. This is commonly observed for the primary body of NEA and small MBA binaries, and suggests that, despite lacking various surface physics effects and irregular shapes, this model captures the bulk re-shaping behavior of these observed asteroids.

Holsapple (2010) investigated the results of slow spin-up using analytical methods, similar to previous work which determined spin-limits and equilibrium shapes for granular materials (Holsapple, 2001, 2007). In the Holsapple (2010) study, it was found that re-shaping actually prevents mass loss, thereby presumably preventing satellite formation. It is possible the "lumpiness" of our numerical models causes this difference in outcome. We note that real asteroids probably are lumpy to some extent (based on observations), and the Holsapple (2010) model cannot actually support mass loss.

Holsapple (2010) suggested that increasing resolution in the *N*-body simulations should produce results approaching their analytical models. Our highest-resolution (5000 particles) simulations do follow a slightly different evolution of axis ratios, but they eventually do evolve towards similar final axis ratios as found in the low resolution simulations (see Fig. 19), and lose mass and accumulate satellites. This is supportive of the explanations for different outcomes in the model provided by Holsapple (2010), and will be the subject of future work. However, the resolution used in this work ($\sim$1000 particles) was selected for the expected constituent size of internal pieces ($\sim$150 m) of a "rubble pile" asteroid ($\sim$3 km) and not strictly for computational reasons (Richardson et al., 2002; Pravec et al., 2002). Thus, exploration of higher-resolution simulations will be of interest in understanding the

Table 2
Summary of the cases of "fission" detected throughout all simulation. The criteria for fission was set at a minimum instantaneous mass loss of 2% of the progenitor's mass, and a prolate (a/c 2.0) progenitor at the time of mass-loss. The cases where more than one fission event occured in the same simulation is denoted by the "–" in the initial a/c and ϕ columns.

a/c (initial)	ϕ	ϵ_N	M_{sec}/M_{pri}	Timesteps (50 s)	a/c (fission)	Rotation (h)
1.0	20	0.2	0.02	1,142,000	2.49	4.33
1.0	20	0.4	0.02	951,000	2.44	4.20
1.0	20	0.4	0.02	1,550,000	2.60	4.17
1.0	20	0.4	0.02	732,000	2.51	4.12
1.0	20	0.4	0.02	1,277,000	2.90	4.62
1.0	20	0.8	0.02	946,000	2.41	4.08
2.0	20	0.2	0.02	1,659,000	2.80	4.51
–	–		0.02	1,794,000	2.64	4.45
1.0	0	0.2	0.04	539,000	2.23	3.88
–	–	0.2	0.02	949,000	2.09	3.48
1.0	0	0.2	0.02	556,000	2.01	3.89
–	–	0.2	0.02	713,000	2.11	3.76
–	–	0.2	0.02	1,613,000	2.12	3.69
1.0	0	0.2	0.07	639,000	1.53	3.13
1.0	0	0.4	0.05	613,000	2.41	4.50
1.0	0	0.4	0.02	489,000	1.70	3.78
–	–	0.4	0.02	567,000	1.85	3.66
2.0	0	0.2	0.02	1,218,000	1.97	4.19
2.0	0	0.2	0.02	1,179,000	1.73	3.58
2.0	0	0.2	0.02	440,000	2.07	4.30
2.0	0	0.2	0.02	1,485,000	2.06	4.02
–	–	0.2	0.02	1,637,000	2.14	4.19
2.0	0	0.2	0.02	1,001,000	1.96	4.23
2.0	0	0.2	0.02	851,000	1.97	4.16
–	–	0.2	0.02	1,677,000	1.84	3.94
2.0	0	0.2	0.02	1,684,000	1.93	4.12
–	–	0.2	0.02	1,684,000	1.43	3.65
2.0	0	0.4	0.03	1,071,000	2.39	5.14
–	–	0.4	0.02	1,588,000	2.10	4.46
–	–	0.4	0.02	1,795,000	2.03	4.13
2.0	0	0.4	0.02	0672,000	1.95	4.28
–	–	0.4	0.02	1,223,000	2.07	4.07
2.0	0	0.4	0.03	1,097,000	2.07	4.11
2.0	0	0.4	0.03	1,743,000	1.80	3.63
2.0	0	0.4	0.03	1,205,000	1.83	4.09
2.0	0	0.4	0.03	0989,000	1.96	4.28
2.0	0	0.4	0.02	1,235,000	1.68	3.88
2.0	0	0.6	0.02	0402,000	2.04	4.25
2.0	0	0.6	0.02	0947,000	1.81	3.93
2.0	0	0.6	0.02	0955,000	1.94	4.21

relationship between analytical models of granular material and *N*-body models, but may not be as relevant to the physical evolution of small asteroids.

Similar models of asteroid re-shaping have recently been explored that have included surface forces, including friction (Sánchez and Scheeres, 2012). These models use a Soft-Sphere Discrete Element Code, which relies on a spring-dashpot representation of contact deformation, approximated by allowing particles to interpenetrate, something that our models did not include (the collisions in our simulations are resolved before particle's overlap; see Sánchez and Scheeres (2011) and Schwartz et al. (2011) for details on the SSDEM algorithms, also note that we are currently testing a similar formulation within `pkdgrav` as described in Schwartz et al., 2011). The inclusion of friction appears to alter the overall behavior of the rubble piles during the spin-up process, resulting in some fission events. Again, we emphasize that our re-shaping simulations found that our nominal bodies behave as if they are granular material with an angle of friction of 40°, and were found to maintain oblate shapes at critical rotation – an essential observed property of NEA binaries (see Fig. 10). A numerical model of a rubble-pile asteroid that cannot maintain an oblate shape at critical rotation is indeed interesting, but may not represent the re-shaping behavior undertaken by the observed binary population of NEAs and small MBAs.

The second limitation is the timescale of the simulations compared to those of the YORP effect. We have attempted to show

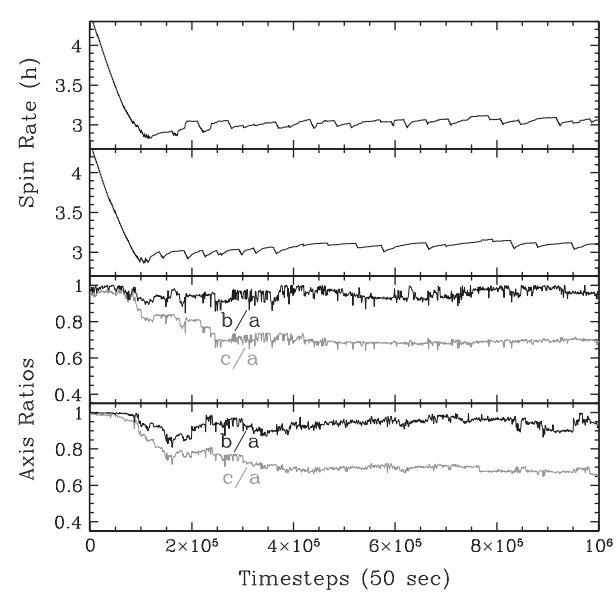

Fig. 18. Comparison of 2000 particle simulations with the 1000 particle nominal case. The evolution of spin rate (upper two panels; topmost is 1000 and second is 2000 particles) and spin axes (lower two panels; same orientation with 1000 particles on top) are plotted against the timestep.

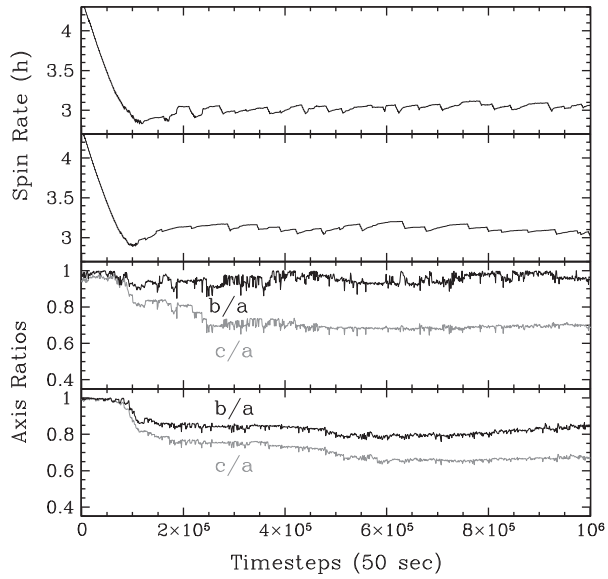

Fig. 19. Comparison of 5000 particle simulations with the 1000 particle nominal case. The evolution of spin rate (upper two panels; topmost is 1000 and second is 5000 particles) and spin axes (lower two panels; same orientation with 1000 particles on top) are plotted against the timestep.

convergence with longer timescale tests, but we are fundamentally limited by computational time. Energy considerations suggest that satellites as small as each of our individual particles (1/1000 mass ratio for a single particle to the rest of the body) have limited lifetimes in their initial orbits due to angular momentum transfer from a non-perfectly-spherical primary (Scheeres (2007)). Similarly, the satellites for known systems are also smaller than these stability criteria from the work of Scheeres (2007), where satellites of 30% the diameter of the primary are ~3% of the system mass. Thus, since all the observations defy the analytical criteria, the issue of particles escaping over longer timescales does not break this model, but rather it suggests the physics involved are more complex than just the criteria found in the rigid body models.

One interpretation of the differences between the analytical criteria and the observations is that the formation process involved more than just 2 bodies. An avalanche or a burst of mass loss would allow a satellite to accumulate in orbit, with an initially low eccentricity, which may help it survive long enough to be observed. Such a burst of mass into low orbit is what was simulated here as a consequence of our limited timescales, but its success in creating systems so similar to the observed population suggests that similar physics may be necessary even at the realistic timescales. Increasing the timescales in the computations is not a feasible method to attack this uncertainty in the model at the current time, so analytical approaches to understanding the many, and sometimes competing, effects of YORP, BYORP and tides will be needed (Ćuk and Burns, 2005; McMahon and Scheeres, 2010b; Ćuk and Nesvorný, 2010; Taylor and Margot, 2010; Goldreich and Sari, 2009). In fact, Jacobson and Scheeres (2011b) have suggested that a balance between the BYORP effect and solid body tides may play a stabilizing role for the observed satellites. This balancing effect may also provide the survival mechanism for the small orbiting pieces as they slowly accumulate into a sizeable satellite. This stabilization method requires that the orbiting debris have synchronous rotation, so that the BYROP effect stays active to balance tides.

5.1. Discussion of the formation of binary asteroids

What are the consequences of these results for the understanding of the observed asteroid population, specifically the population of binaries? We attempt to list the most relevant observations that need to be reconciled with any model(s) of binary formation:

(i) The apparent YORP produced binary population among NEAs and small MBAs, and their properties (this population is sometimes refered to as "asynchronous" despite commonly being in synchronous spin states). These account for the large majority of discovered binaries in these populations (~32/35), and have very generic characteristic properties (see Section 1.3). These binaries account for ~15% of all NEAs and small MBAs. The observations typically provide precise measurements of primary spin rate and separation, and a very reliable measurement of the primary equatorial elongation (b/a).
(ii) The best observed binary NEA, 1999 KW_4, which has a shape model for both components and well-defined orbital properties. It is the proto-type of the YORP binary population, and is particularly noteworthy due to the "top-shape" of its primary – a shape which is becoming ubiquitous among this class of asteroids.
(iii) The observed triple asteroids in the NEA population, 2001 SN_{263}, and 1994 CC, which have properties similar to the YORP binary population with the addition of the distant outer satellite
(iv) The observed fraction of asteroids with bifurcated mass distributions, sometimes refered to as "contact-binaries", is estimated to be around ~10%.
(v) The minority of observed binaries among NEAs and small MBAs; those with nearly similar-sized components, which are occasionally doubly synchronous e.g., Hermes, Berna, or Tama.
(vi) The population of "split" binary pairs in the Main Belt: recently discovered asteroids with nearly-identical orbits which are estimated to have been bound in the recent past.

Given our current knowledge of the YORP effect and the properties of observed binary systems, the presented scenario of spin-up leading to mass loss and secondary formation in orbit is a viable candidate for the formation of the YORP binary population (i). The properties of the systems are a close match, and it provides a generic and efficient process that explains the similarity of the systems observed and the high estimated fractions. Among NEAs, 2/3 of fast rotators (periods between 2.2 and 2.8 h), are such binaries (Pravec et al., 2006). Thus, if the YORP effect increases the rotation rate of asteroids and instigates mass loss and satellite formation, then it must be very efficient once the spin-up process begins – meaning that once the progenitor gets to a rapid rotation rate (faster than 2.8 h for example) it typically continues all the way to satellite formation rather than stalling out very near the critical spin limit. This could be in part due to the short timescales involved, with YORP doubling timescales being estimated at anywhere from 10^4 to 10^6 years, which is small compared to the 10^7 year dynamical lifetime of NEAs. This means that rarely are objects observed in the process of spinning up. However, this work shows that some significant reshaping of the body could precede mass loss and would likely continue throughout mass loss. Multiple studies have shown that the magnitude of the YORP effect is very sensitive to small-scale features or the internal mass-distribution of the asteroids (Statler, 2009; Scheeres and Gaskell, 2008). It is still unclear what fraction of asteroids are currently experiencing, have previously experienced, or will in the future experience spin-state alteration due to the YORP effect. The spin rate distribution of small asteroids is well-explained by large-scale alteration of spin states by YORP, so it is necessary that many, or most, are evolving by YORP (Pravec et al., 2008; Rossi et al., 2009). Therefore, asteroids that are spun-up to near-critical levels, but do not progress to

satellite formation, may simply start spinning down and not contribute to a noticeable population of "failed binaries" or asteroids with rapid rotation but no satellite.

It is also unclear how the shape changes described in this work would alter the on-going spinup; would each minute shape-change randomly reset the YORP state, creating a random walk effect (Statler, 2009; Scheeres and Gaskell, 2008)? Or does some intrinsic property of the body keep it spinning up to mass loss and binary formation? A random-walk of spin-state changes might seemingly prevent the process described in this work, as many small shape-changes and mass-loss events that are a natural part of this process would each require a random re-setting of the bodies YORP state. This may lead to a mechanism that requires the minimal number of shape changes and mass loss events, in order to avoid a YORP-change that stops satellite growth. However, this problem also afflicts the case in which each satellite is directly placed into orbit in a single mass loss event. In this case the primary loses significant angular momentum at the moment of mass-loss, and thus still requires additional YORP spinup to regain a spin state near-critical – after a dramatic shape change during the loss of its satellite. It also requires that the primary somehow takes the generic oblate shape that is observed (with 1999 KW_4 as the prototype), or it has to reshape again to reach that shape. Therefore escaping this potential pitfall of random-walk YORP resetting is problematic for many different proposed formation mechanisms.

The primaries in these simulations naturally have rapid rotation due to the continued spin increases, and they end up with the oblate shape that is observed directly for 1999 KW_4. This matches the observations, though less directly as most observed primary shapes are estimated via the low lightcurve amplitudes measured for the primaries of the rest of the population (ii). The final size and orbits of the secondaries are determined by whichever evolutionary mechanism slows or stops the original YORP spinup e.g., tides or BYORP. The secondaries stop growing when the YORP-effect stops the spin-up and mass-loss of the primary, and the presented simulations find that the secondaries are naturally in close orbits, though this could be a function of the shortened timescales. Ćuk (2007) postulates that secondaries reaching ~30% the size of the primary will start to be dominated by Binary-YORP effect, which could be the shutoff mechanism responsible for stopping satellite growth in the size ranges observed. Other studies of BYORP also suggest that this mechanism is capable of removing the same secondary on very short timescales, so the overall role of BYORP is still a matter of debate (McMahon and Scheeres, 2010b). Binaries with a slowly spinning primary are decidedly not observed; so primaries either do not have their rotation rate slowed by YORP, or secondaries are quickly lost when a primary's rotation rate begins slowing.

The best-studied triple asteroid in the NEA population fits neatly into the YORP binary group if only its inner satellite is considered (iii), due to the size ratio, primary spin and primary shape. Thus it appears possible that it has undergone the described satellite formation in the presence of a pre-existing outer satellite (which itself could have been formed similarly through YORP spin-up and then evolved outward through BYORP or tides). However, this is not directly tested in this work, and the formation/evolution of the outer satellite is not easy to explain. The outermost satellite is distant enough that normal solid body tides are likely incapable of circularizing its orbit on Solar System timescales (Walsh and Richardson, 2006), and might be the first observed system which requires BYORP to be explained. A new study attempts to build a comprehensive model of binary and triple asteroid formation via the YORP-effect via fission of solid components into orbit (Jacobson and Scheeres, 2011a). This work has the advantage of using rigid-body formulations to integrate very long timescales, but lack the fundamental re-shaping aspect provided by a particle code as presented in this work. Jacobson and Scheeres (2011a) do present a possible solution for triple asteroids as the result of an initial secondary fissioning after reaching critical rotation due to gravitational torques of the primary. This same secondary fission process is also suggested as a means to account for the consistent shapes seen among nearly all well-observed NEA binary objects.

The appealing aspect of the separation of two distinct components of a binary is that presumably only minimal re-shaping would occur before the near-instantaneous formation/release of the secondary. This eases, but does not eliminate, the concern about the YORP-effect being shut-off by the constant reshaping found in the presented work (even in these scenarios, the large pieces move relative to the primary before "lifting off", as well there might require post-disruption spin-up and re-shaping to achieve observed spin rates and shapes among primaries). However, matching all of the consistent properties of the YORP binary population is a difficult aspect of relying on separation of two components and would likely require a post-formation primary-reshaping/spin-up process to explain the very consistent properties of the observed population. The split binary population (vi) found in the Main Belt has been modeled as a natural outcome from the process of separation of contact binaries, representing separation that has failed to remain bound (Pravec et al., 2010). This population does not overlap with the properties of the YORP binaries as they have much more variation in lightcurve amplitude for the primaries (or larger bodies in the case of split pairs) and cover a substantially wider range of size ratio. The work of Pravec et al. (2010) shows that direct fission due to YORP is active in the Solar System, but does not directly explain the consistent and generic properties of the observed YORP binaries. The population of binaries with similar sized components (v), the "Hermes" class, may be related to this group and eventually explained with the same mechanism (Jacobson and Scheeres, 2011a).

Similarly, formation of binaries from contact binaries (iv) demands a population of contact binaries (currently estimated to be ~9% (Benner et al., 2006)). When a contact binary is forced into a YORP spinup cycle there are only three possible outcomes: forming a stable binary, evolving back to a contact-binary, or splitting. Then a fair question is how do we replenish the source population of contact binaries, since two of the three possible outcomes eliminate them?

Our model provides an explanation for the formation of the YORP binary asteroids that is consistent with observations. Rubble-pile asteroids are generically capable of reshaping and undergoing piece-wise mass loss and satellite formation if they enter a YORP cycle and spin-up to critical rotation rates. Some will spin down, filling the slow rotator excess, and others may never be YORP active at all. The population of contact binaries could potentially be created, replenished or expanded by the variety of evolutionary effects acting on the formed binaries. Together the fractions of binaries, contact binaries and slow rotators may represent a steady state of a very YORP-active population of bodies which are frequently undergoing spin state alterations on very short timescales, an idea that has in fact been invoked to explain the distribution of spin rates among NEAs (Pravec et al., 2008; Rossi et al., 2009), and also utilized by Jacobson and Scheeres, 2011a to explain binaries, triples, contact-binaries and split binaries.

Acknowledgments

KJW was supported by the Henri Poincaré fellowship at the Observatoire de la Côte d'Azur, Nice, France. PM had the support of the French Programme National de Planetologie. DCR acknowledges support of the National Aeronautics and Space Administration under Grant No. NNX08AM39G issued through the Office of Space Science and by the National Science Foundation under Grant

No. AST0708110. We acknowledge the use of the Mesocentré de Calcul-SIGAMM at the Observatoire de la Côte d'Azur and the borg cluster at the University of Maryland.

References

Behrend, R. et al., 2006. Four new binary minor planets: (854) Frostia, (1089) Tama, (1313) Berna, (4492) Debussy. Astron. Astrophys. 446, 1177–1184.

Benner, L.A.M., Nolan, M.C., Ostro, S.J., Giorgini, J.D., Pray, D.P., Harris, A.W., Magri, C., Margot, J.L., 2006. Near-Earth Asteroid 2005 CR37: Radar images and photometry of a candidate contact binary. Icarus 182, 474–481.

Binney, J., Tremaine, S., 1987. Galactic Dynamics. Princeton University Press, Princeton, NJ, 747.

Bottke, W.F., Vokrouhlicky, D., Rubincam, D.P., Nesvorny, D., 2006. The yarkovsky and yorp effects: Implications for asteroid dynamics. Annu. Rev. Earth Planet. Sci. 34, 157–191.

Brozović, M., Benner, L.A.M., Taylor, P.A., Nolan, M.C., Howell, E.S., Magri, C., Scheeres, D.J., Giorgini, J.D., Pollock, J.T., Pravec, P., Galád, A., Fang, J., Margot, J.L., Busch, M.W., Shepard, M.K., Reichart, D.E., Ivarsen, K.M., Haislip, J.B., Lacluyze, A.P., Jao, J., Slade, M.A., Lawrence, K.J., Hicks, M.D., 2011. Radar and optical observations and physical modeling of triple near-Earth Asteroid (136617) 1994 CC. Icarus 216, 241–256.

Ćuk, M., 2007. Formation and destruction of small binary asteroids. Astrophys. J. 659, L57–L60.

Ćuk, M., Burns, J., 2005. Effects of thermal radiation on the dynamics of binary neas. Icarus 176, 418–431.

Ćuk, M., Nesvorný, D., 2010. Orbital evolution of small binary asteroids. Icarus 207, 732–743.

Delbo, M., Walsh, K., Mueller, M., Harris, A.W., Howell, E.S., 2011. The cool surfaces of binary near-Earth asteroids. Icarus 212, 138–148.

Durech, J. et al., 2008. Detection of the yorp effect in Asteroid (1620) geographos. Astron. Astrophys. 489, L25–L28.

Goldreich, P., Sari, R., 2009. Tidal evolution of rubble piles. Astrophys. J. 691, 54–60.

Harris, A.W., 1996. The rotation rates of very small asteroids: Evidence for 'rubble pile' structure. Lunar Planet. Sci., 493 (abstracts).

Harris, A.W., Warner, B.D., Pravec, P., 2008. Asteroid lightcurve derived data v10.0. NASA Planetary Data System 95. Dataset editor.

Holsapple, K., 2001. Equilibrium configurations of solid cohesionless bodies. Icarus 154, 432–448.

Holsapple, K., 2004. Equilibrium figures of spinning bodies with self-gravity. Icarus 172, 272–303.

Holsapple, K., 2007. Spin limits of Solar System bodies: From the small fast-rotators to 2003 el61. Icarus 187, 500–509.

Holsapple, K.A., 2010. On YORP-induced spin deformations of asteroids. Icarus 205, 430–442.

Jacobson, S.A., Scheeres, D.J., 2011a. Dynamics of rotationally fissioned asteroids: Source of observed small asteroid systems. Icarus 214, 161–178.

Jacobson, S.A., Scheeres, D.J., 2011b. Long-term stable equilibria for synchronous binary asteroids. Astrophys. J. 736, L19–L23.

Kaasalainen, M., Ďurech, J., Warner, B.D., Krugly, Y.N., Gaftonyuk, N.M., 2007. Acceleration of the rotation of Asteroid 1862 Apollo by radiation torques. Nature 446, 420–422.

Leinhardt, Z.M., Richardson, D.C., 2005. A fast method for finding bound systems in numerical simulations: Results from the formation of asteroid binaries. Icarus 176, 432–439.

Leinhardt, Z.M., Richardson, D.C., Quinn, T., 2000. Direct n-body simulations of rubble pile collisions. Icarus 146, 133.

Lowry, S.C. et al., 2007. Direct detection of the asteroidal yorp effect. Science 316, 272–274.

Masiero, J., Jedicke, R., Ďurech, J., Gwyn, S., Denneau, L., Larsen, J., 2009. The thousand asteroid light curve survey. Icarus 204, 145–171.

McMahon, J., Scheeres, D., 2010a. Detailed prediction for the BYORP effect on binary near-Earth Asteroid (66391) 1999 KW4 and implications for the binary population. Icarus 209, 494–509.

McMahon, J., Scheeres, D., 2010b. Secular orbit variation due to solar radiation effects: A detailed model for BYORP. Celest. Mech. Dynam. Astron. 106, 261–300.

Ostro, S.J. et al., 2006. Radar imaging of binary near-Earth Asteroid (66391) 1999 kw4. Science 314, 1276–1280.

Paddack, S.J., Rhee, J.W., 1975. Rotational bursting of interplanetary dust particles. Geophys. Res. Lett. 2, 365.

Pravec, P., 2000. Fast and slow rotation of asteroids. Icarus 148, 12–20.

Pravec, P., Harris, A., 2007. Binary asteroid population1. Angular momentum content. Icarus 190, 250–259.

Pravec, P., Harris, A.W., Michalowski, T., 2002. Asteroid rotations. Asteroids III, 113–122.

Pravec, P., Scheirich, P., Kusnirak, P., Sarounova, L., Mottola, S., Hahn, G., Brown, P., Esquerdo, G., Kaiser, N., Krzeminski, Z., 2006. Photometric survey of binary near-Earth asteroids. Icarus 181, 63–93.

Pravec, P., Harris, A., Vokrouhlicky, D., Warner, B., Kusnirak, P., Hornoch, K., Pray, D., Higgins, D., Oey, J., Galad, A., 2008. Spin rate distribution of small asteroids. Icarus 197, 497–504.

Pravec, P. et al., 2010. Formation of asteroid pairs by rotational fission. Nature 466, 1085–1088 (1009.2770).

Richardson, D.C., Bottke, W.F., Love, S.G., 1998. Tidal distortion and disruption of Earth-crossing asteroids. Icarus 134, 47–76.

Richardson, D.C., Quinn, T., Stadel, J., Lake, G., 2000. Direct large-scale n-body simulations of planetesimal dynamics. Icarus 143, 45–59.

Richardson, D.C., Leinhardt, Z.M., Melosh, H.J., Bottke, W.F., Asphaug, E., 2002. Gravitational aggregates: Evidence and evolution. Asteroids III, 501–515.

Richardson, D., Elankumaran, P., Sanderson, R., 2005. Numerical experiments with rubble piles: Equilibrium shapes and spins. Icarus 173, 349–361.

Richardson, D., Michel, P., Walsh, K., 2009. Numerical simulations of asteroids modelled as gravitational aggregates with cohesion. Planet. Space Sci. 57, 193–200.

Rossi, A., Marzari, F., Scheeres, D.J., 2009. Computing the effects of YORP on the spin rate distribution of the NEO population. Icarus 202, 95–103.

Rubincam, D., 2000. Radiative spin-up and spin-down of small asteroids. Icarus 148, 2–11.

Sánchez, P., Scheeres, D.J., 2011. Simulating asteroid rubble piles with a self-gravitating soft-sphere distinct element method model. Astrophys. J. 727, 120.

Sánchez, P., Scheeres, D.J., 2012. DEM simulation of rotation-induced reshaping and disruption of rubble-pile asteroids. Icarus. doi:10.1016/j.icarus.2012.01.014.

Scheeres, D.J., 2007. Rotational fission of contact binary asteroids. Icarus 189, 370–385.

Scheeres, D., Gaskell, R., 2008. Effect of density inhomogeneity on YORP: The case of Itokawa. Icarus 198, 125–129.

Schwartz, S.R., Richardson, D.C., Michel, P., Walsh, K.J., 2011. Modeling the granular surface and interior of small bodies using the soft-sphere discrete element method: Implementation in the N-body code pkdgrav and tests. In: EPSC-DPS Joint Meeting 2011, p. 1240.

Slivan, S.M., 2002. Spin vector alignment of Koronis family asteroids. Nature 419, 49–51.

Statler, T.S., 2009. Extreme sensitivity of the YORP effect to small-scale topography. Icarus 202, 502–513.

Steinberg, E., Sari, R., 2011. Binary YORP effect and evolution of binary asteroids. Astron. J. 141, 55.

Taylor, P.A., Margot, J.L., 2010. Tidal evolution of close binary asteroid systems. Bull. Am. Astron. Soc. 925.

Taylor, P.A. et al., 2007. Spin rate of Asteroid (54509) 2000 PH5 increasing due to the YORP effect. Science 316, 274–277.

Vokrouhlický, D., Nesvorný, D., Bottke, W.F., 2003. The vector alignments of asteroid spins by thermal torques. Nature 425, 147–151.

Walsh, K., Richardson, D., 2006. Binary near-Earth asteroid formation: Rubble pile model of tidal disruptions. Icarus 180, 201–216.

Walsh, K., Richardson, D., 2008. A steady-state model of nea binaries formed by tidal disruption of gravitational aggregates. Icarus 193, 553–566.

Walsh, K.J., Richardson, D.C., Michel, P., 2008. Rotational breakup as the origin of small binary asteroids. Nature 454, 188–191.